

Short range inter-vortex interaction and interacting dynamics of half-quantized vortices in two-component Bose-Einstein condensates

Kenichi Kasamatsu¹, Minoru Eto², and Muneto Nitta³

¹*Department of Physics, Kinki University, Higashi-Osaka, 577-8502, Japan*

²*Department of Physics, Yamagata University, Yamagata 990-8560, Japan*

³*Department of Physics, and Research and Education Center for Natural Sciences, Keio University, Hiyoshi 4-1-1, Yokohama, Kanagawa 223-8521, Japan*

(Dated: March 1, 2022)

We study the interaction and dynamics of two half-quantized vortices in two-component Bose-Einstein condensates. Using the Padé approximation for the vortex core profile, we calculate the intervortex potential, whose asymptotic form for a large distance has been derived by Eto *et al.* [Phys. Rev. A, **83**, 063603 (2011)]. Through numerical simulations of the two-dimensional Gross-Pitaevskii equations, we reveal different kinds of dynamical trajectories of the vortices depending on the combinations of signs of circulations and the intercomponent density coupling. Under the adiabatic limit, we derive the equations of motion for the vortex coordinates, in which the motion is caused by the balance between Magnus force and the intervortex forces. The initial velocity of the vortex motion can be explained quantitatively by this point vortex approximation, but understanding the long-time behavior of the dynamics needs more consideration beyond our model.

PACS numbers: 03.75.Lm, 03.75.Mn, 67.85.Fg

I. INTRODUCTION

Exotic topological defects are interesting subjects in various physical area from condensed matter physics to high energy physics [1]. Among them these topological defects, exotic vortices, e.g., half-quantized vortices (HQVs) or more generally fractional vortices [2], can appear in the systems of multicomponent order parameters. HQVs have been discussed in various area of physics [3], and recently they have been observed experimentally in triplet superconductors [4], exciton-polariton condensates [5, 6], ultracold atomic gas Bose-Einstein condensates (BECs) [7], and helium 3 superfluids [8]. Among them quantized vortices in multicomponent BEC are one of the important subjects [9, 10].

Quantized vortices in cold atomic BECs have been studied thoroughly since its experimental realization [11]. The recent progress in this subject can be seen in development of the techniques to nucleate the vortices and to detect the real time vortex dynamics. The group of Amherst College demonstrated the observation of real time evolution of a single vortex, a vortex dipole, and a cluster of a few vortices in a single-component BEC [12–14]. These experimental observation was compared with the simple intuitive theories of the point vortex approximation, where the vortex motion is described by fundamental equations of the vortex positions and the interaction between point vortices.

Two-component BECs are a simplest example of the multicomponent condensates and have also attracted much interest to study the novel phenomena not found in a single component BEC. The mass circulation of two-component BECs is fractionally quantized when their mass densities are different. Such a quantized vortex in two-component BECs has a composite structure, where a vortex core in one component is filled by the density of

the other component [10, 15–18]. This vortex structure was created experimentally through coherent interconversion between two components [19].

Recently, the asymptotic form of the interaction between two HQVs in two-component BECs was derived analytically, having the form $\sim (\ln R)/R^2$ for HQVs separated by a large distance R [20]. This R -dependence is different from that of the vortex-vortex interaction $\sim \ln R$ in a single-component BEC [21]. Since the two components interact only through the density-density coupling, the vortex in one component does not directly feel the circulation of the vortex in the other component. This fact results in an indirect interaction of the HQVs, where the filling component of each vortex core is affected by the circulation created by the vortex in the same component, dragging the vortex in which it is filled by the intercomponent density-density coupling. While the vortex interaction in a scalar BEC depends on the circulations of each vortex, the interaction for the HQVs does not depend on the sign of the circulation but on the sign and magnitude of the intercomponent coupling. Aftalion *et al.* studied the equilibrium properties of multi-vortex systems in two-component BECs using the above asymptotic form [22], and some studies have discussed the vortex-vortex interaction beyond the asymptotic regime [23, 24].

A next question naturally arises as how two interacting HQVs behave temporally. Although the real time dynamics of two vortices in two-component BECs was studied numerically by Öhberg and Santos [25], they considered only particular situations in a harmonically trapped system. Nakamura *et al.*, studied the n -vortex dynamics in multicomponent BECs through the variational analysis and the resulting equations of motions for the vortex positions are shown to include the terms of inertial vortex mass [26], which are usually neglected in the case of vortex motion in a scalar BEC.

In this paper, we study the real time evolution of the two interacting HQVs in homogeneous two-component BEC. We find that depending on not only the vortex interaction but also the signs of circulation of the HQVs, the vortex motions exhibit interesting nontrivial trajectories. We consider the vortex dynamics for two cases (i) one of two vortices is placed in either of the two components and (ii) two vortices are placed in the same component. For the case (i), even though the intervortex interaction is independent of the sign of circulation, the dynamical trajectories of two vortices are different for the signs as well as for the intercomponent coupling strength. In the case (ii), the dynamics also has nontrivial dependence on the intercomponent coupling. The initial stage of the dynamics can be explained by the classical equations of motions for the point vortices, where it is important to take account of the short-range property of the vortex-vortex interaction.

This paper is organized as follows. Section II is devoted for representing the basic formulation of the following numerical simulations and the analytical calculations. In Sec. III, we consider the interaction and dynamics of two vortices, in which one of these is put on either of the two components. We study the interacting dynamics by directly solving the two-dimensional Gross-Pitaevskii (GP) equations for two-component BECs. We interpret the numerical results by handling the point vortex approximation, finding that the proper treatment of the short range force between the two vortices can explain the short time behavior of the numerical results. We also consider the dynamics for two vortices which are put on the one of the two components in Sec. IV using similar treatments in Sec. III. Summary and discussions are presented in Sec. V.

II. VORTICES IN TWO-COMPONENT BOSE-EINSTEIN CONDENSATES

In this section, we give the theoretical formulation to study the vortex dynamics in two-component BECs. Usually, atomic condensates are trapped by harmonic traps, which give rise to the density inhomogeneity with an inverted parabolic form. Such an inhomogeneity has significant influence to vortex dynamics [11]. Since we are willing to consider the intrinsic dynamics caused by the vortex-vortex interaction, we restrict ourselves to the homogeneous system. This situation is realistic because a recent experiment demonstrated a realization of degenerate Bose gases in a uniform box potential [27].

A. The Gross-Pitaevskii model

We start with the Lagrangian for homogeneous two-component BEC systems

$$L = \int d\mathbf{r} \left\{ \sum_{i=1,2} \left[-\frac{i\hbar}{2} (\Psi_i \dot{\Psi}_i^* - \Psi_i^* \dot{\Psi}_i) - \frac{\hbar^2}{2m_i} |\nabla \Psi_i|^2 - \mu_i |\Psi_i|^2 - \frac{g_i}{2} |\Psi_i|^4 \right] - g_{12} |\Psi_1|^2 |\Psi_2|^2 \right\}, \quad (1)$$

where Ψ_i is a condensate wave function of the i -th component ($i = 1, 2$) with the mass m_i and the chemical potential μ_i . The coupling constants g_1, g_2 and g_{12} represent the atom-atom interactions proportional to the s -wave scattering length; the Ψ_1 and Ψ_2 components repel or attract for $g_{12} > 0$ or $g_{12} < 0$, respectively. We restrict ourselves to the miscible situation, where the equilibrium densities without vortices are $n_{10} = (\mu_1 g_2 - \mu_2 g_{12}) / (g_1 g_2 - g_{12}^2)$ and $n_{20} = (\mu_2 g_1 - \mu_1 g_{12}) / (g_1 g_2 - g_{12}^2)$. To normalize the equation, we introduce the scales of length and time by $\xi = \sqrt{\hbar^2 / 2m_1 \mu_1}$ and $\hbar / \mu_1 = \tau$. Replacing $t / \tau \rightarrow t$, $\mathbf{r} / \xi \rightarrow \mathbf{r}$, and $\Psi_i = \sqrt{n_{i0}} \psi_i$, we then get

$$\tilde{L} = \int d\mathbf{r} \left\{ -\frac{i}{2} (\psi_1 \dot{\psi}_1^* - \psi_1^* \dot{\psi}_1) - \frac{i}{2} \tilde{\gamma} (\psi_2 \dot{\psi}_2^* - \psi_2^* \dot{\psi}_2) - [|\nabla \psi_1|^2 + \alpha \tilde{\gamma} |\nabla \psi_2|^2 + \frac{c_1}{2} (|\psi_1|^2 - 1)^2 + \frac{c_2}{2} \tilde{\gamma} (|\psi_2|^2 - 1)^2 + c_2 \gamma (|\psi_1|^2 - 1) (|\psi_2|^2 - 1)] \right\}, \quad (2)$$

where $\tilde{L} = L / \mu_1 n_{10} \xi^2$ and the parameters are given by

$$c_1 = \frac{g_1 n_{10}}{\mu_1}, \quad c_2 = \frac{g_2 n_{20}}{\mu_1}, \quad \alpha = \frac{m_2}{m_1}, \quad \tilde{\gamma} = \frac{n_{20}}{n_{10}}, \quad \gamma = \frac{g_{12}}{g_2}. \quad (3)$$

In these scales, the equilibrium amplitude of the wave function becomes $|\psi_1| = |\psi_2| = 1$. For simplicity, the parameters in the following discussion are put as $m_1 = m_2 = m$, $\mu_1 = \mu_2 = \mu$ and $g_1 = g_2 = g$, and thus $n_{10} = n_{20}$. Then, the parameters in Eq. (3) become $\alpha = 1$, $c_1 = c_2 = (1 + \gamma)^{-1}$, and $\tilde{\gamma} = 1$. The free parameter γ has a range $-1 < \gamma < 1$.

The coupled GP equations are obtained by the variational principle of the action with the Lagrangian Eq. (2) as (note that $\mu = 1$ in our unit)

$$i \frac{\partial \psi_1}{\partial t} = \left(-\nabla^2 - 1 + \frac{1}{1 + \gamma} |\psi_1|^2 + \frac{\gamma}{1 + \gamma} |\psi_2|^2 \right) \psi_1, \quad (4)$$

$$i \frac{\partial \psi_2}{\partial t} = \left(-\nabla^2 - 1 + \frac{1}{1 + \gamma} |\psi_2|^2 + \frac{\gamma}{1 + \gamma} |\psi_1|^2 \right) \psi_2. \quad (5)$$

The stationary coupled GP equations can be derived by

neglecting the time dependence:

$$\left(-\nabla^2 + \frac{1}{1+\gamma}|\psi_1(\mathbf{r})|^2 + \frac{\gamma}{1+\gamma}|\psi_2(\mathbf{r})|^2\right)\psi_1(\mathbf{r}) = \psi_1(\mathbf{r}), \quad (6)$$

$$\left(-\nabla^2 + \frac{1}{1+\gamma}|\psi_2(\mathbf{r})|^2 + \frac{\gamma}{1+\gamma}|\psi_1(\mathbf{r})|^2\right)\psi_2(\mathbf{r}) = \psi_2(\mathbf{r}). \quad (7)$$

B. Half-quantized vortex

Since there are miscible binary condensates in space where the condensate wave functions $\psi_i = \sqrt{\rho_i}e^{i\theta_i}$ are defined, two $U(1)$ symmetries are spontaneously broken in the system. Accordingly, the order parameter space is

$$T^2 \simeq U(1)_1 \times U(1)_2 \simeq \frac{U(1)_{\text{mass}} \times U(1)_{\text{spin}}}{\mathbb{Z}_2}. \quad (8)$$

Here, each $U(1)_i$ ($i = 1, 2$) corresponds to the phase rotation of ψ_1 or ψ_2 , while $U(1)_{\text{mass}}$ and $U(1)_{\text{spin}}$ correspond to the overall and relative phase rotations, defined by

$$\Theta = (\theta_1 + \theta_2)/2, \quad \phi = (\theta_1 - \theta_2)/2 \quad (9)$$

that transform as

$$\begin{aligned} U(1)_{\text{mass}} : \quad & \psi_1 \rightarrow \psi_1 e^{i\alpha}, \quad \psi_2 \rightarrow \psi_2 e^{i\alpha}, \quad \Theta \rightarrow \Theta + 2\alpha \\ U(1)_{\text{spin}} : \quad & \psi_1 \rightarrow \psi_1 e^{i\beta}, \quad \psi_2 \rightarrow \psi_2 e^{-i\beta}, \quad \phi \rightarrow \phi + 2\beta \end{aligned} \quad (10)$$

whose currents are mass and pseudo-spin currents, respectively.

The gradient of these angles can be regarded as a mass and a spin current, respectively. Since both the condensates ψ_1 and ψ_2 are unchanged under the \mathbb{Z}_2 action defined by $\alpha = \beta = \pi$ inside $U(1)_{\text{mass}} \times U(1)_{\text{spin}}$ in Eq. (10), this \mathbb{Z}_2 has to be removed as the denominator of Eq. (8). If the only ψ_1 -component has a vortex $\psi_1 = \sqrt{\rho_1}e^{i\theta}$ with the polar angle θ , the pseudo-spinor of the order parameter can be written as

$$\begin{pmatrix} \psi_1 \\ \psi_2 \end{pmatrix} = \begin{pmatrix} \sqrt{\rho_1}e^{i\theta} \\ \sqrt{\rho_2} \end{pmatrix} = \sqrt{\rho}e^{i\theta/2} \begin{pmatrix} \zeta_1 e^{i\theta/2} \\ \zeta_2 e^{-i\theta/2} \end{pmatrix}, \quad (11)$$

where $\zeta_1^2 + \zeta_2^2 = 1$. In terms of $U(1)_{\text{mass}}$ and $U(1)_{\text{spin}}$ in Eq. (10), the both angles Θ and ϕ are rotated by π with circling around a vortex. Since this vortex can be seen as having a half winding of $U(1)_{\text{mass}}$, it is often called a *half-quantized vortex* (HQV). The first prediction in the context of atomic-gas BEC was given by Leonhardt and Volovik [9]. These similar structures have been predicted in thin films of superfluid $^3\text{He-A}$ [3], and observed for both exciton-polariton BECs [5, 6] and chiral p -wave superconductors [4].

The structure of a simple HQV located on the origin of the space along the z -axis can be obtained by solving

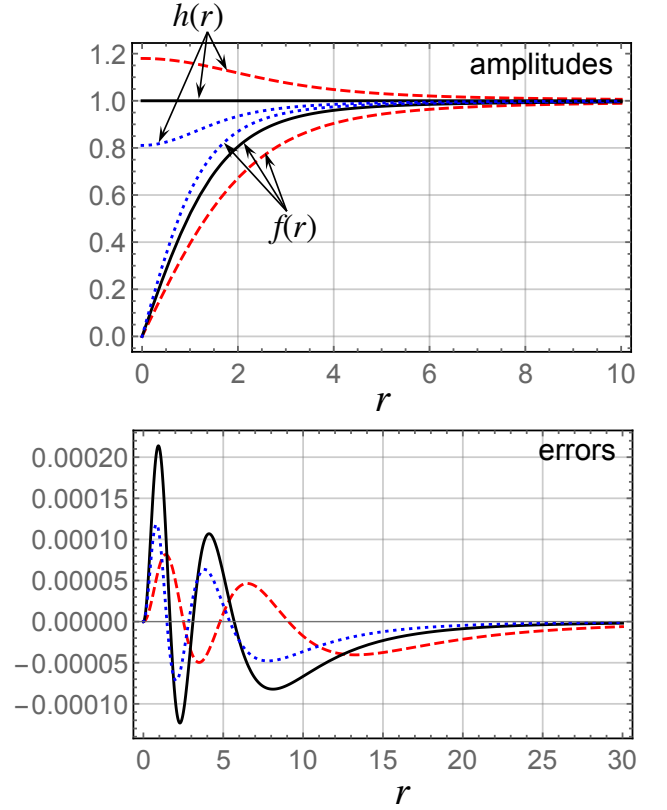


FIG. 1. (Color online) The numerical solutions for $f(r)$ and $h(r)$ with $\gamma = 0.5$ (red long-dashed curves), 0 (black solid curves), and -0.5 (blue short dashed curves) are shown in the upper panel. The lower panel are plots of the error of the Padé approximation from the numerical solutions: $(f_{\text{num}} - f_{\text{Padé}})/f_{\text{num}}$. The style of plotting curves corresponds to the one in the upper panel.

Eqs. (6) and (7) with an ansatz for an axially symmetric configuration

$$\psi_1 = \sqrt{f(r)}e^{i\theta}, \quad \psi_2 = \sqrt{h(r)}, \quad (12)$$

where (r, θ) is the polar coordinate and we assume that ψ_1 has a vortex with the winding number 1 and ψ_2 is vortex-free. Typical numerical solutions are shown in Fig. 1. A universal feature of configuration is that the profile function h of unwinding field at the vortex center is concave for $g_{12} < 0$ and convex for the $g_{12} > 0$. This can be understood from the atom-atom interaction g_{12} ; in the presence of the vortex profile for ψ_1 as a background, ψ_2 feels the potential $g_{12}|\psi_1|^2$ and it tends to be trapped in the vortex center for the repulsive interaction $g_{12} > 0$ and to be exclusive from the vortex center for the attractive interaction $g_{12} < 0$. When ψ_2 has a vortex and ψ_1 is vortex free, the role of f and h in Eq. (12) is exchanged.

Although the solution can be obtained only by numerically, it is practical to use the approximate analytical form of the profile f and h for calculating the physi-

TABLE I. List of the values of the parameters in Eqs. (14) and (15) as a function of γ .

| γ | a_1 | a_2 | a_3 | b_1 | b_2 | a_0 | b_0 |
|----------|----------|----------|----------|----------|----------|----------|----------|
| -0.9 | 0.258405 | 1.001440 | 0.128055 | 0.677999 | 0.231094 | 0.893941 | 0.302519 |
| -0.8 | 0.288090 | 0.887745 | 0.043337 | 0.632548 | 0.207753 | 0.746991 | 0.415541 |
| -0.7 | 0.328417 | 0.845890 | 0.034572 | 0.604638 | 0.185217 | 0.658306 | 0.505052 |
| -0.6 | 0.331510 | 0.810535 | 0.044151 | 0.583411 | 0.164030 | 0.592318 | 0.583911 |
| -0.5 | 0.320207 | 0.778227 | 0.054746 | 0.565440 | 0.143665 | 0.538307 | 0.657000 |
| -0.4 | 0.301442 | 0.746212 | 0.059707 | 0.549184 | 0.123534 | 0.491584 | 0.726859 |
| -0.3 | 0.279456 | 0.714102 | 0.059945 | 0.533788 | 0.102964 | 0.449661 | 0.795066 |
| -0.2 | 0.256806 | 0.682365 | 0.057508 | 0.518693 | 0.080933 | 0.411045 | 0.862748 |
| -0.1 | 0.234548 | 0.651120 | 0.053656 | 0.503478 | 0.055062 | 0.374758 | 0.930797 |
| 0.0 | 0.212942 | 0.620126 | 0.049024 | — | — | 0.340110 | — |
| 0.1 | 0.191892 | 0.588923 | 0.043910 | 0.050700 | 0.468493 | 0.306585 | 1.071106 |
| 0.2 | 0.171146 | 0.556895 | 0.038440 | 0.068459 | 0.448235 | 0.273774 | 1.144887 |
| 0.3 | 0.150382 | 0.523257 | 0.032653 | 0.079615 | 0.426540 | 0.241333 | 1.222194 |
| 0.4 | 0.129252 | 0.487011 | 0.026562 | 0.086596 | 0.402814 | 0.208962 | 1.304013 |
| 0.5 | 0.107461 | 0.446909 | 0.020237 | 0.090117 | 0.376227 | 0.176376 | 1.391547 |
| 0.6 | 0.084925 | 0.401450 | 0.013950 | 0.090202 | 0.345525 | 0.143300 | 1.486338 |
| 0.7 | 0.061980 | 0.348770 | 0.008304 | 0.086311 | 0.308600 | 0.109448 | 1.590464 |
| 0.8 | 0.039332 | 0.285410 | 0.003955 | 0.077039 | 0.261349 | 0.074514 | 1.706916 |
| 0.9 | 0.017902 | 0.201664 | 0.000913 | 0.058583 | 0.193295 | 0.038159 | 1.840424 |

cal quantities such as the intervortex potential. Their asymptotic form for large r is known as [20]

$$f(r) \sim 1 - \frac{1}{(1-\gamma)r^2}, \quad h(r) \sim 1 + \frac{\gamma}{(1-\gamma)r^2}. \quad (13)$$

The miscible condition of the ground state ensures that the denominator is always positive for each of Eqs. (13), while $h(r)$ changes its sign when $\gamma < 0$. Recently, a variational ansatz of a HQV that describes well around its vortex core was considered by Mason [28], but it does not reproduce the asymptotic form for large r . Here, we apply the Padé approximation to the profile function as

$$f(r) = \frac{a_0 r^2 + a_1^2 r^4 + a_3^2 (1-\gamma) r^6}{1 + a_2^2 r^2 + (a_1^2 + a_3^2) r^4 + a_3^2 (1-\gamma) r^6}, \quad (14)$$

$$h(r) = \begin{cases} \frac{b_0 + (b_1^2 + b_2^2) r^2 + b_1^2 [(1-\gamma)/\gamma] r^4}{1 + b_2^2 r^2 + b_1^2 [(1-\gamma)/\gamma] r^4} & \text{for } \gamma > 0, \\ \frac{b_0 + b_1^2 r^2 + b_2^2 [(\gamma-1)/\gamma] r^4}{1 + (b_1^2 + b_2^2) r^2 + b_2^2 [(\gamma-1)/\gamma] r^4} & \text{for } \gamma < 0, \end{cases} \quad (15)$$

where these functional forms are determined so as to reproduce the asymptotic form of Eq. (13) for large r . The parameters in Eqs. (14) and (15) are determined by fitting them to the numerical solution, especially the behavior of the solution starting from $r = 0$. The values are summarized in Table I. The error from the numerical solutions is within the range $\pm 0.02\%$ as shown in Fig. 1. For $\gamma = 0$, Eq. (15) reduces to $h = 1$.

In the following, we denote the vortex state as (q_1, q_2) , where a vortex with the winding number q_1 (q_2) in ψ_1 (ψ_2)-component at a certain position \mathbf{r} . Since we consider two vortices located in different positions, we will use the notation, e.g., $(q_1, 0)$ - $(0, q_2)$, where one vortex with q_1 -winding in ψ_1 is positioned at \mathbf{r}_1 and the other with

q_2 -winding in ψ_2 is positioned at \mathbf{r}_2 . We restrict ourselves to a single circulation $q_i = \pm 1$. The $(1, 0)$ - $(0, \pm 1)$ state represents that one of two vortices is put on the different positions in either of the two components, and the $(1, 0)$ - $(\pm 1, 0)$ state represents that two vortices are put on the different positions in one of the two components.

III. VORTEX DYNAMICS FOR $(1, 0)$ AND $(0, \pm 1)$

A. Intervortex interaction

First, we look back to the properties of intervortex interaction between two HQVs. The asymptotic form of the intervortex interaction for well separated vortices has been calculated by Eto *et al.* [20]. In this work, we include the short range behavior of the intervortex potential based on the approximation form of Eqs. (14) and (15). We assume that the wave function with two vortices can be described by simply multiplying the two single vortex profiles at different positions, referred to as the Abrikosov ansatz, as

$$\begin{aligned} \psi_1 &= \sqrt{\rho_1} e^{i\theta_1} = \sqrt{f(\mathbf{r} - \mathbf{r}_1) h(\mathbf{r} - \mathbf{r}_2)} e^{iq_1 \theta^0(\mathbf{r} - \mathbf{r}_1)}, \\ \psi_2 &= \sqrt{\rho_2} e^{i\theta_2} = \sqrt{h(\mathbf{r} - \mathbf{r}_1) f(\mathbf{r} - \mathbf{r}_2)} e^{iq_2 \theta^0(\mathbf{r} - \mathbf{r}_2)} \end{aligned} \quad (16)$$

with the two phase singularities at the point $\mathbf{r}_1 = (R, 0)$ and $\mathbf{r}_2 = (-R, 0)$ as

$$\theta^0(x \pm R, y) = \arctan \frac{x \pm R}{y}. \quad (17)$$

Inserting the ansatz Eqs. (16) to the total energy

$$E_0^{(q_1, q_2)} = \int d\mathbf{r} \left\{ \sum_{i=1,2} \left[\frac{(\nabla \rho_i)^2}{4\rho_i} + \rho_i (\nabla \theta_i)^2 + \frac{(\rho_i - 1)^2}{2(1 + \gamma)} \right] + \frac{\gamma}{1 + \gamma} (\rho_1 - 1)(\rho_2 - 1) \right\}, \quad (18)$$

we can calculate the intervortex potential from the relation [20]

$$V_{12}(r_{12}) = E_0^{(1,1)} - E_0^{(1,0)} - E_0^{(0,1)} + E_0^{(0,0)}, \quad (19)$$

where $r_{12} = |\mathbf{r}_2 - \mathbf{r}_1| = 2R$ and Eq. (18) means $E_0^{(0,0)} = 0$.

For a certain value of γ , we calculate Eq. (18) using the profile function Eqs. (14) and (15) with the parameters displayed in Table I. The integration was done numerically because the direct integration by hand yields complicated form according to Eqs. (14) and (15). The plot of V_{12} for $\gamma = 0.5$ and -0.5 is shown in Fig. 2. The vortex interaction is repulsive and attractive for $\gamma > 0$ and $\gamma < 0$, respectively. For large R , the potential behaves as the asymptotic form derived by Ref. [20]:

$$V_{12}^{\text{asy}}(r_{12}) = \frac{4\pi\gamma}{1 - \gamma} \frac{\log(r_{12}/2\xi_{\text{cut}})}{r_{12}^2}. \quad (20)$$

Here, ξ_{cut} is an uncertain cut-off length, which is determined by the fitting to the result by numerical integration of Eq. (19) for large R [20]; the values for $\gamma = \pm 0.5$ are written in the caption of Fig. 2. The numerical result matches the asymptotic form even for a short distance (down to $R \simeq 5$). Especially, the potential for negative γ shows a good agreement. Thus, we can say from this analysis that the asymptotic form of Eq. (20) describes V_{12} well even for a short distance between two vortices. The deviation becomes significant for $\gamma \rightarrow 1$, because the vortex core extends over the space so that the description of the asymptotic form becomes worse.

B. Numerical simulations

Here, we study the dynamics of two interacting vortices in two-component BECs by numerically solving the time-dependent GP equations (4) and (5). The initial state is prepared as follows. We first put the vortices using the Abrikosov ansatz with the approximated profile of Eqs. (14) and (15) as well as the phase profile Eq. (17) at $x = +R$ in the ψ_1 -component and at $x = -R$ in the ψ_2 -component. Using this wave function, we obtain the more accurate initial configuration through the short imaginary time evolution of Eqs. (4) and (5). This procedure can remove some numerical error associated with the approximation function Eqs. (14) and (15), which improve the accuracy of the following real time simulations. During this imaginary time evolution, the position of the phase singularities moves but its displacement is very small. We impose the Neumann condition to the

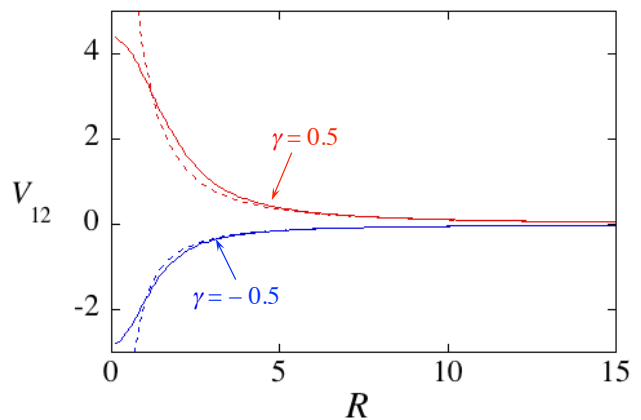


FIG. 2. (Color online) The intervortex potential Eq. (19) as a function of R for $\gamma = 0.5$ and $\gamma = -0.5$. The solid curve represents the results by numerical integration of Eq. (18) with the approximated vortex profile Eqs. (14) and (15), while the dashed curve represents the asymptotic form of Eq. (20) with $\xi_{\text{cut}} = 0.30$ for $\gamma = 0.5$ and $\xi_{\text{cut}} = 0.18$ for $\gamma = -0.5$.

numerical boundary. The size of the numerical box is $[-40, +40]$ in unit of ξ and the grid number is 512×512 [29].

1. The same circulation: (1,0)-(0,1) vortex

In this subsection, we focus on the dynamics of the HQVs with the same circulation, namely (1,0)-(0,1). The typical vortex trajectories in the simulation is shown in Figs. 3 and 4; only the trajectory of the vortex in the ψ_1 -component is shown because that of the ψ_2 -component is symmetric with respect to the origin. For $\gamma < 0$, each vortex makes a closed quasi-circular trajectory as shown in Fig. 3. With increasing the separation R , the velocity of the motion becomes longer and the trajectory is gradually distorted from the circular shape. The distortion occurs in such a way that the radius of the circular motion is reduced. We see that these behaviors are qualitatively similar to the cases with different values of γ , but there are some quantitative differences, e.g., the velocity of motion becomes slightly faster as $|\gamma|$ is increased.

For $\gamma > 0$, each vortex also makes a quasi-circular trajectory as shown in Fig. 4, but the initial velocity is inverted to that in the $\gamma < 0$ cases. In this case, the trajectory is also distorted with increasing R in such a way that the radius of the circular motion is slightly expanded. For the initial separation larger than $R \simeq 4$, the vortices go away by getting off the closed trajectory. The velocity of motion is also monotonically decreased (increased) with R (γ).

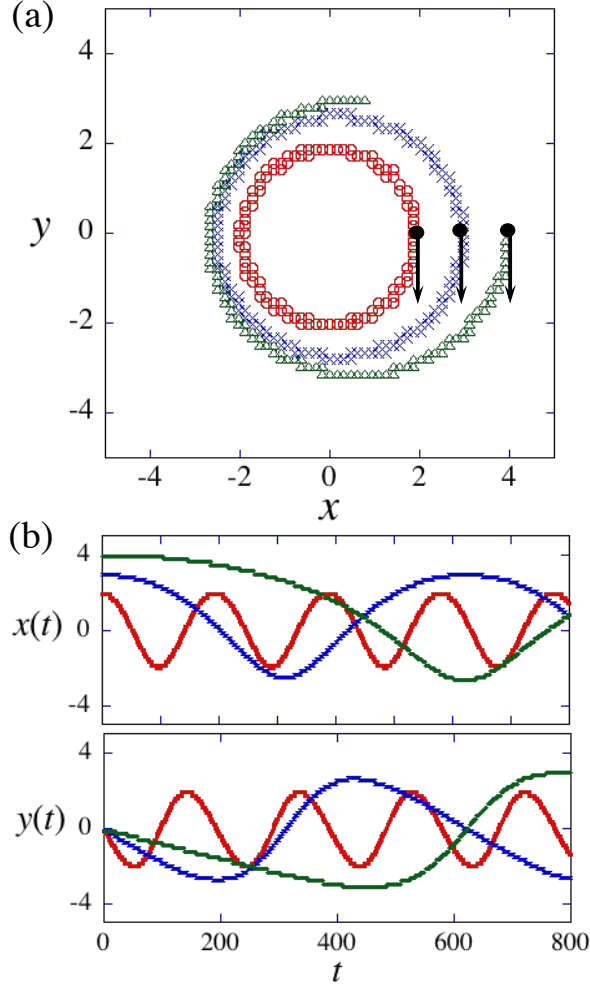


FIG. 3. The vortex motion of two HQVs with the same circulation for $\gamma = -0.5$, where one of the two vortices are put on either of the two components, i.e., $(1, 0)$ - $(0, 1)$. The panels (a) shows the vortex trajectories for ψ_1 -component for the time $[0, 800]$. The (red) circles, (blue) cross, and (green) triangles represents the results for initial separation $R = 2, 3$, and 4 . The initial position and the direction of the motion are indicated by black dots and arrows, respectively. The vortex trajectory of the ψ_2 -component is symmetric with respect to the origin. The bottom panels (b) represent the time evolution of the vortex coordinate $x(t)$ (top) and $y(t)$ (bottom) in the ψ_1 -component.

2. The different circulation: $(1, 0)$ - $(0, -1)$ vortex

Next, we study the dynamics of two HQVs with opposite circulations $(1, 0)$ and $(0, -1)$. It is known that an usual vortex-anti-vortex pair (vortex dipole) in a single-component BEC goes straightforwardly by keeping the distance between a vortex and an anti-vortex. However, the dynamics of a pair of a HQV and an anti-HQV is remarkably different.

Figure 5 shows the trajectories for $\gamma < 0$. Since the

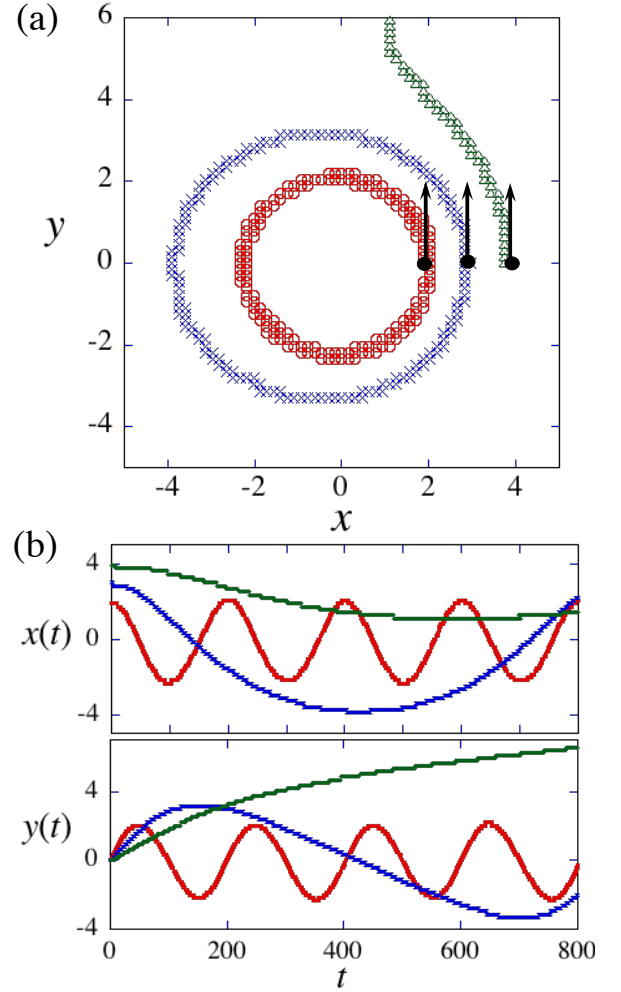


FIG. 4. The vortex motion of two HQVs with the same circulation $(1, 0)$ - $(0, 1)$ for $\gamma = 0.5$. The plots are similar to Fig. 3.

vortex trajectories in the two components are symmetric with respect to the y -axis, we only show those in the ψ_1 -component. The vortices in each component initially move to the same negative y -direction, but their separation gradually decreases. The vortices eventually touch each other but they are not annihilated as known in a pair annihilation of a vortex dipole in a single-component BEC. After that, they exchange their positions, go back to the positive y -direction and touch each other again. This motion continues and forms a closed trajectory. The velocity of the vortex motion becomes slower with increasing the initial separation R . We can see that the trajectories for $R = 3$ and 4 approach to that for $R = 2$, which implies the existence of a stable trajectory around $R = 2$.

The results for $\gamma > 0$ are shown in Fig. ???. Although both vortices initially move to the positive y -direction linearly, they are gradually apart from each other and eventually go back to the negative y -direction. As R

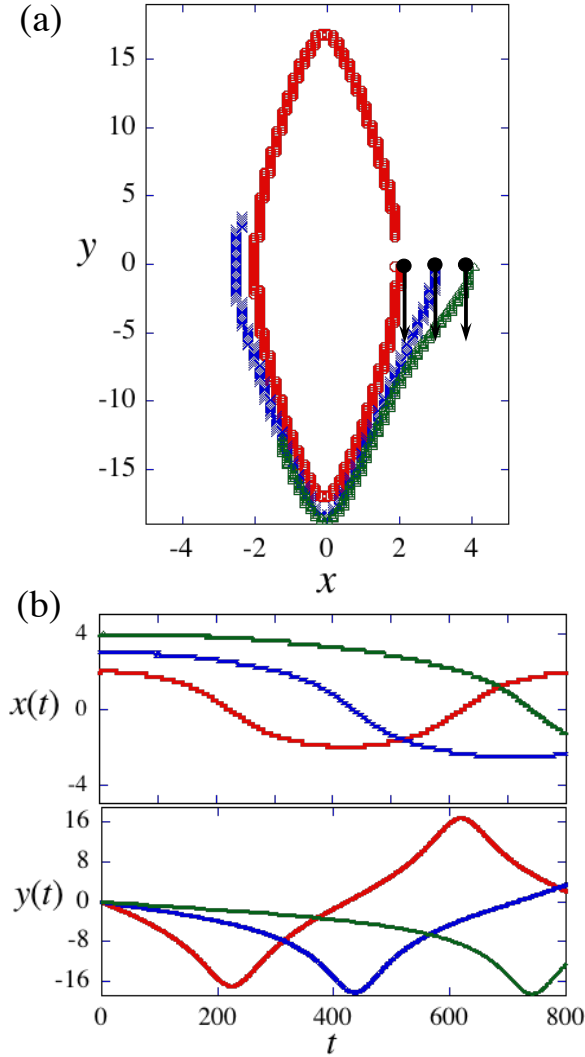


FIG. 5. The vortex motion of two HQVs with $(1, 0)$ - $(0, -1)$ for $\gamma = -0.5$, where the initial vortex separation is $R = 2, 3, 4$. Since the vortex trajectories in the two components are symmetric with respect to the y -axis, we only show those in the ψ_1 -component in (a). The notation is similar with Fig. 3.

increases, the initial velocity of motion becomes slower and the deviation from the linear trajectory takes place soon.

C. Point vortex approximation

To understand the physical origin observed in the numerical simulations in Sec. III B, we consider the dynamics of two HQVs using a point vortex approximation. This approximation is valid when the vortex core size is small so that the vortex can be seen as a point. To our knowledge, use of this model is not established for the dynamics of HQVs in two-component BEC. As shown below, our point vortex approximation can provide cor-

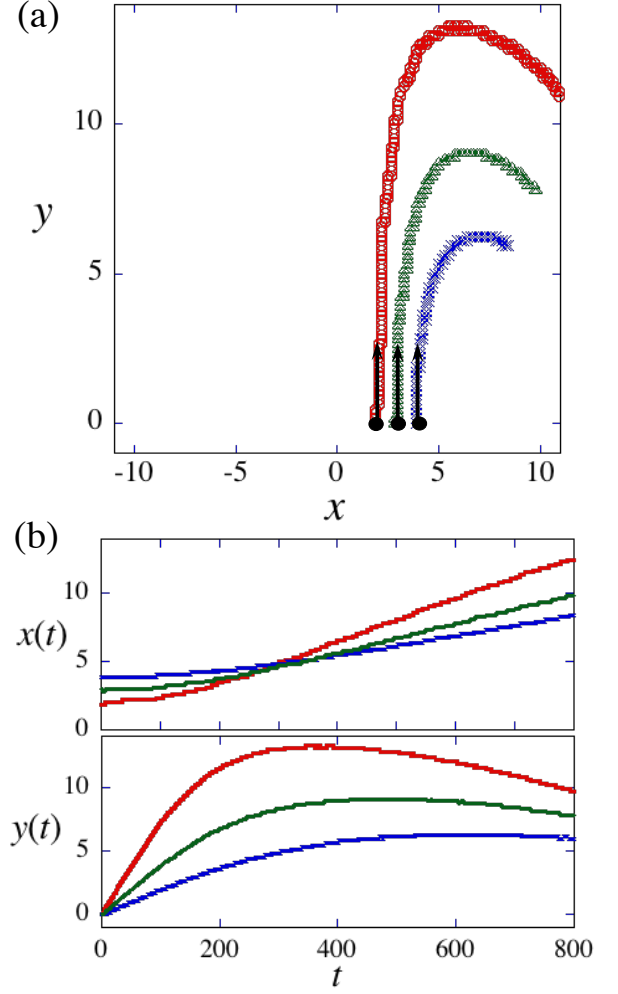


FIG. 6. The plots similar to Fig. 5 for $\gamma = 0.5$.

rect results only to the early stage of the dynamics, so that we need additional treatment to understand the full dynamics.

We give the Abrikosov ansatz and the adiabatic approximation for the wave function of the i -th component

$$\psi_i(\mathbf{r}, t) = \sqrt{\rho_i(\mathbf{r}, \mathbf{r}_1(t), \mathbf{r}_2(t))} e^{i\theta_i(\mathbf{r}, t, \mathbf{r}_i(t))}, \quad (21)$$

where

$$\rho_1(\mathbf{r}, \mathbf{r}_1(t), \mathbf{r}_2(t)) = f(\mathbf{r} - \mathbf{r}_1(t))h(\mathbf{r} - \mathbf{r}_2(t)), \quad (22)$$

$$\theta_1(\mathbf{r}, t, \mathbf{r}_1(t)) = q_1\theta^0(\mathbf{r} - \mathbf{r}_1(t)), \quad (23)$$

$$\rho_2(\mathbf{r}, \mathbf{r}_1(t), \mathbf{r}_2(t)) = h(\mathbf{r} - \mathbf{r}_1(t))f(\mathbf{r} - \mathbf{r}_2(t)), \quad (24)$$

$$\theta_2(\mathbf{r}, t, \mathbf{r}_2(t)) = q_2\theta^0(\mathbf{r} - \mathbf{r}_2(t)). \quad (25)$$

Here, the amplitudes f and h represent the core profiles of the HQV, approximately given by Eqs. (14) and (15), and $\mathbf{r}_i(t) = (x_i(t), y_i(t))$ denotes the vortex position. The two HQVs have the same density profile because of the symmetric choice of our parameters. The above ansatz

means that two vortices are well separated and each vortex keeps its shape as a single vortex solution even during the dynamics. We expect that the density fluctuations such as phonons would have a minor effect for the vortex dynamics and thus neglect them. The phase has a profile of the vortex winding

$$\theta^0(\mathbf{r} - \mathbf{r}_i(t)) = \arctan \left[\frac{y - y_i(t)}{x - x_i(t)} \right]. \quad (26)$$

By substituting the ansatz Eqs. (21)-(25) to the Lagrangian

$$L = - \int d\mathbf{r} [\rho_1 \dot{\theta}_1 + \rho_2 \dot{\theta}_2] - E_0^{(q_1, q_2)}, \quad (27)$$

we can derive the Euler-Lagrange equations for the vortex coordinates $\mathbf{r}_i(t)$. After some calculations, the equations of motion can be written as

$$2\pi q_1 \dot{y}_1 = - \frac{\partial V_{12}}{\partial x_1}, \quad (28)$$

$$-2\pi q_1 \dot{x}_1 = - \frac{\partial V_{12}}{\partial y_1}, \quad (29)$$

$$2\pi q_2 \dot{y}_2 = - \frac{\partial V_{12}}{\partial x_2}, \quad (30)$$

$$-2\pi q_2 \dot{x}_2 = - \frac{\partial V_{12}}{\partial y_2}. \quad (31)$$

Here, V_{12} represents the inter-vortex potential given by Eq. (19). The details of the derivation are described in the Appendix A. The equations are essentially similar to those used in a single-component system [13, 14], where the vortex motion can be described by the balance between the Magnus force and the intervortex force.

The properties of the vortex motions depend on the sign of q_i . Let us see the case for the $(1,0)$ - $(0,1)$ vortex $[(q_1, q_2) = (1, 1)]$. One can show that $\mathbf{r}_1 + \mathbf{r}_2$ is a constant of motion. For the symmetric initial position such as $x_2(0) = -x_1(0)$ as in our simulations, the above constants are zero and the relative distance r_{12} is also time-independent. Thus, we obtain the equation of motion for \mathbf{r}_i as

$$\ddot{\mathbf{r}}_i = - \left[\frac{1}{\pi r_{12}} \frac{\partial V_{12}}{\partial r_{12}} \right]^2 \mathbf{r}_i. \quad (32)$$

This represents an uniform circular motion and the rotation frequency depends on the γ . From Eq. (28), the initial velocity $\dot{y}_1(0)$ is positive (negative) for $\gamma > 0$ ($\gamma < 0$), which is consistent with the numerical results.

For the $(1,0)$ - $(0,-1)$ vortex $[(q_1, q_2) = (1, -1)]$, one can show that $\mathbf{r}_1 - \mathbf{r}_2$ is a constant of motion. For an appropriate choice of the initial condition such as $x_1(0) - x_2(0) = 2R$ and $y_1(0) - y_2(0) = 0$ as in our simulations, the solution is given by

$$\begin{aligned} x_1 &= R, & x_2 &= -R \\ y_1 &= y_2 = \frac{1}{2\pi} \left(\frac{\partial V_{12}}{\partial r_{12}} \right) t. \end{aligned} \quad (33)$$

This is exactly an uniform linear motion for both vortices. The initial velocity $\dot{y}_1(0)$ is positive (negative) for $\gamma > 0$ ($\gamma < 0$), which is also consistent with the numerical results.

Therefore, the vortex point model can explain partly the numerical results, but cannot describe some observed dynamics, namely, the deviation from the circular trajectory seen in Figs. 3 and 4 as well as the deviation from the linear trajectory in Figs. 5 and 6. Understanding these observation would need more effects beyond the ansatz Eqs. (21)-(25).

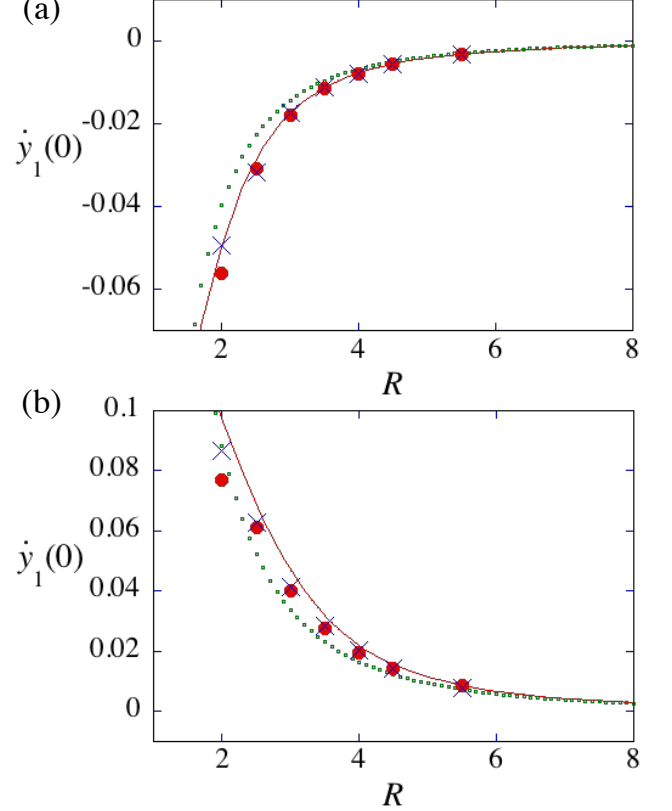


FIG. 7. The comparison of the initial velocity of the HQV in the ψ_1 -component between the numerical simulations and evaluation from the intervortex force by using the Abrikosov ansatz (a) $\gamma = -0.5$ and (b) $\gamma = 0.5$. We plot the initial velocity $\dot{y}(0)$ as a function of the initial separation R . The (red) circles and (blue) crosses represent the numerical results of the GP equation for $(1,0)$ - $(0,1)$ and $(1,0)$ - $(0,-1)$, respectively. The initial velocity is estimated by the linear fit of the short time behavior of $y_1(t)$ from $t = 0$. The solid curve represents $(\partial V_{12}/\partial r_{12})/2\pi$, where V_{12} is calculated from Eq. (19) with the approximated profile function of Eqs. (14) and (15). The dotted curve corresponds to the results obtained from the asymptotic intervortex interaction Eq. (20): $\dot{y}_1(0) = \frac{\gamma}{q_1(1-\gamma)} \frac{2 \ln(R/\xi_{\text{cut}}) - 1}{4R^3}$ with $q_1 = +1$.

According to Eqs. (28)-(31), the qualitative properties of vortex motion depend only on the circulation of the vortices, being independent of the intervortex interac-

tion. The intervortex interaction determines the initial velocities of the vortices. The initial direction of the vortex motion is determined by the sign of γ , while the magnitude of the initial velocity is dependent on the value of γ irrespective of the sign of q_i . We compare the initial velocity of y_1 obtained from the intervortex force calculated from both the asymptotic potential Eq. (20) and the numerical integration of Eq. (19) with those obtained in the numerical simulations, which is shown in Fig. 7. For $R \geq 6$ the vortex motion becomes quite slow and it is difficult to obtain an accurate velocity from the numerical data. The numerical results agree very well with the initial velocity obtained by the numerical integration of Eq. (19) for $\gamma < 0$, while for $\gamma > 0$ the numerical results are slightly deviated from that in the range $R \leq 4$. This can be explained by including the neglected terms when we derive Eqs. (28)-(31), which will be discussed in the Appendix B. Therefore, the initial stage of the dynamics can be captured by the vortex-point model Eqs. (28)-(31). The asymptotic form of the intervortex potential approximately works well even for a short distance between two vortices.

IV. VORTEX DYNAMICS FOR (1,0)-($\pm 1,0$)

A. Intervortex potential

Next, we consider the vortex interaction and dynamics when the two vortices are put in the same component, say ψ_1 -component, along with the procedure similar to the previous section.

First, we consider the intervortex potential. It is known that for well separated vortices at $\mathbf{r}_1 = (R, 0)$ and

$\mathbf{r}_2 = (-R, 0)$ in a single-component BEC the intervortex interaction is given by [21]

$$V_{12} = 2\pi \ln \frac{R^2 + \Lambda^2}{4R^2}. \quad (34)$$

Here, we use the scale ξ and τ to get the dimensionless form of the potential and Λ is the system size. For (1,0)-($\pm 1,0$) states of two-component BECs, the vortex interaction should be modified by the presence of inter-component interaction. However, Eto *et al.* [20] showed that, using the asymptotic form Eq. (13) of the vortex profile, the intervortex interaction is independent of the γ , namely g_{12} , being given by Eq. (34) for the leading order of the vortex separation.

We expect that the γ -dependence may appear in the short range property of the intervortex potential. We thus calculate the intervortex potential without using the asymptotic form. The simple Abrikosov ansatz for the wave function is given by

$$\begin{aligned} \psi_1 &= \sqrt{f(\mathbf{r} - \mathbf{r}_1)f(\mathbf{r} - \mathbf{r}_2)} e^{iq_1\theta^0(\mathbf{r}-\mathbf{r}_1)+iq_2\theta^0(\mathbf{r}-\mathbf{r}_2)}, \\ \psi_2 &= \sqrt{h(\mathbf{r} - \mathbf{r}_1)h(\mathbf{r} - \mathbf{r}_2)} \end{aligned} \quad (35)$$

where f and h are given by Eqs. (14) and (15). However, for nearly approaching vortices, the simple Abrikosov ansatz does not work in this situation, because two (1,0)-(1,0) vortices must be converted to a vortex with double winding number in the first component (2,0), and two (1,0)-(-1,0) vortices must be annihilated for vanishing separation $R = 0$. Thus, we have to consider a more suitable ansatz of the vortex profile to reproduce this situation. For (1,0)-(1,0) state we can introduce the improved Abrikosov ansatz following the work [30] as

$$\psi_1 = (z - z_1)(z - z_2) \left[\epsilon_1 \frac{\sqrt{f(\mathbf{r} - \mathbf{r}_1)f(\mathbf{r} - \mathbf{r}_2)}}{|\mathbf{r} - \mathbf{r}_1||\mathbf{r} - \mathbf{r}_2|} + (1 - \epsilon_1) \frac{\sqrt{F(r)}}{r^2} \right], \quad (36)$$

$$\psi_2 = \epsilon_2 \sqrt{h(\mathbf{r} - \mathbf{r}_1)h(\mathbf{r} - \mathbf{r}_2)} + (1 - \epsilon_2) \sqrt{H(r^*)} \quad (37)$$

with $z = x + iy$, $\mathbf{r}_1 = (R, 0)$ and $\mathbf{r}_2 = (-R, 0)$. Here, $F(\mathbf{r})$ and $H(\mathbf{r})$ represent the profile function of the double-quantized vortex and the corresponding unwinding field, respectively. Using the Padé approximation, we obtain these profile functions as

$$F(r) = \frac{A_0 r^4 + A_1^2 r^6 + [A_2^2(1 - \gamma)/4] r^8}{1 + A_3^2 r^2 + A_4^2 r^4 + (A_1^2 + A_2^2) r^6 + [A_2^2(1 - \gamma)/4] r^8}, \quad (38)$$

$$H(r) = \begin{cases} \frac{B_0 + B_2^2 r^2 + (B_1^2 + B_4^2) r^4 + B_1^2 [(1 - \gamma)/4\gamma] r^6}{1 + B_3^2 r^2 + B_4^2 r^4 + B_1^2 [(1 - \gamma)/4\gamma] r^6} & \text{for } \gamma > 0, \\ \frac{B_0 + B_2^2 r^2 + B_1^2 r^4 + B_4^2 [(\gamma - 1)/4\gamma] r^6}{1 + B_3^2 r^2 + (B_1^2 + B_4^2) r^4 + B_4^2 [(\gamma - 1)/4\gamma] r^6} & \text{for } \gamma < 0. \end{cases} \quad (39)$$

As done in Sec. II B, the parameters are determined by the fitting to the numerical solutions, as listed in Ta-

ble II. The parameters $\epsilon_{1,2}$ represent the weight between the first and second terms, being determined variation-

ally; $\epsilon_{1,2} = 1$ reproduces an asymptotic configuration of the separated vortices, while $\epsilon_{1,2} = 0$ does the $(2, 0)$ vortex. Thus, Eqs. (36) and (37) nicely improve the simple Abrikosov ansatz around zero vortex separation $R = 0$. Concrete values of $\epsilon_{1,2}$ are shown in Fig. 8.

In the second term the factor $|z^2 - R^2|/r^2$ has the effect of replacing the double zero of F at the origin with two zeros at $z = \pm R$. Because of this change of the zero points in ψ_1 , we also modify the profile of H by replacing $r \rightarrow r^* \equiv \sqrt{|\mathbf{r} - \mathbf{r}_1||\mathbf{r} - \mathbf{r}_2|}$. Using these profile functions, we substitute the ansatzs Eqs. (36) and (37) to the total energy and find the optimal values of ϵ_1 and ϵ_2 . As expected, this optimal $\epsilon_{1,2}$ are small for small R , but quickly approaches to 1 as R increases past a value of ≈ 4 , as shown in Fig. 8.

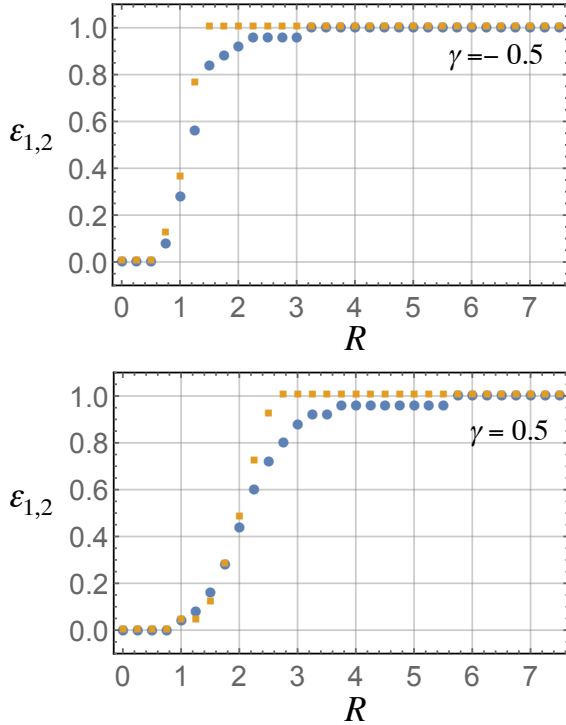


FIG. 8. (Color online) The variational parameters ϵ_1 (blue circles) and ϵ_2 (yellow squares) for $\gamma = -0.5$ (upper panel) and $\gamma = 0.5$ (lower panel). The horizontal axes are vortex separations R .

In Fig. 9, we plot the intervortex potential as a function of R , where we calculate V_{12} using the simple Abrikosov ansatz Eq. (35). For the $(1, 0)$ - $(1, 0)$ vortex, we also calculate with the improved ansatz Eqs. (36) and (37); we do not consider such an improvement of ansatz for the $(1, 0)$ - $(-1, 0)$ case. The potential is slowly decaying function with increasing in R and asymptotically described by Eq. (34). We can confirm that the potential has a γ -dependance in a short distance. When we use the improve Abrikosov ansatz, the increase in V_{12} for $R \rightarrow 0$ is strongly suppressed. A plateau appears at $R = 0$, and

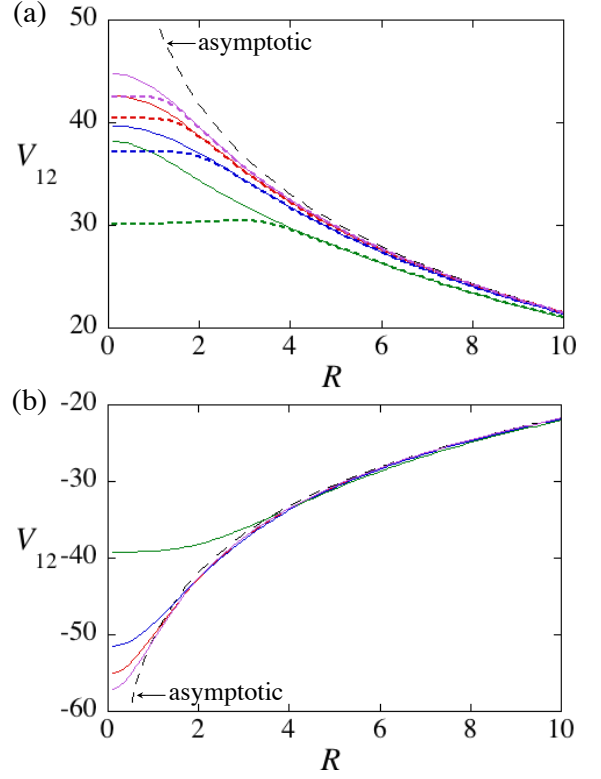


FIG. 9. (Color online) The intervortex potential for (a) $(1, 0)$ - $(1, 0)$ and (b) $(1, 0)$ - $(-1, 0)$ case, as a function of the vortex separation R . The plots correspond to V_{12} for $\gamma = -0.4, 0, 0.4, 0.8$ from top to bottom curves in (a) and vice versa for (b). In (a), the results obtained by two different methods are distinguished by the solid (simple Abrikosov) and the bold-dashed (improved Abrikosov) curves. In (b), we only show the result of the simple Abrikosov ansatz. The asymptotic potential Eq. (34) is also plotted by a thin-dashed curve for both (a) and (b).

moreover V_{12} seems to form a local minimum at $R = 0$ for γ near 1. However, as seen below, this local minimum is a consequence of the breakdown of the ansatz Eqs. (36) and (37) around an intermediate region between the coincident vortices and well-separated vortices.

B. Numerical simulations

Next, we consider the vortex motion by directly solving the GP equation. The initial state is prepared as the similar way in Sec. III B. However, during the short imaginary time evolution, the vortices tend to move repulsively for the $(1, 0)$ - $(1, 0)$ case and attractively for the $(1, 0)$ - $(-1, 0)$ case. Thus, we stop the evolution when the vortices come to the expected position.

TABLE II. List of the values of the parameters in Eqs. (38) and (39) as a function of γ .

| γ | A_1 | A_2 | A_3 | A_4 | B_1 | B_2 | B_3 | B_4 | A_0 | B_0 |
|----------|----------|----------|----------|----------|----------|----------|----------|----------|----------|----------|
| -0.9 | 0.000000 | 0.044085 | 0.655626 | 0.361754 | 0.174282 | 0.286248 | 0.369131 | 0.027326 | 0.123596 | 0.168104 |
| -0.8 | 0.069187 | 0.030517 | 0.628252 | 0.328574 | 0.153605 | 0.297146 | 0.359327 | 0.032409 | 0.095082 | 0.274568 |
| -0.7 | 0.086909 | 0.028872 | 0.635450 | 0.312520 | 0.139898 | 0.301351 | 0.349658 | 0.030685 | 0.078140 | 0.370791 |
| -0.6 | 0.085943 | 0.031564 | 0.626964 | 0.294624 | 0.129413 | 0.302121 | 0.339959 | 0.027272 | 0.065735 | 0.462552 |
| -0.5 | 0.075776 | 0.032859 | 0.599957 | 0.272692 | 0.120663 | 0.300841 | 0.330249 | 0.023438 | 0.055808 | 0.552190 |
| -0.4 | 0.064181 | 0.031788 | 0.567658 | 0.249943 | 0.112920 | 0.298138 | 0.320411 | 0.019539 | 0.047479 | 0.640957 |
| -0.3 | 0.054056 | 0.029371 | 0.536912 | 0.228342 | 0.105771 | 0.294312 | 0.310305 | 0.015658 | 0.040294 | 0.729641 |
| -0.2 | 0.045799 | 0.026410 | 0.509087 | 0.208299 | 0.098960 | 0.289497 | 0.299789 | 0.011749 | 0.033992 | 0.818786 |
| -0.1 | 0.034307 | 0.023979 | 0.467809 | 0.187238 | 0.092311 | 0.283730 | 0.288728 | 0.007576 | 0.028408 | 0.908799 |
| 0 | 0.032810 | 0.020333 | 0.457036 | 0.171538 | — | — | — | — | 0.023439 | — |
| 0.1 | 0.000515 | 0.083379 | 0.388462 | 0.334831 | 0.006105 | 0.269140 | 0.264375 | 0.078768 | 0.019014 | 1.092646 |
| 0.2 | 0.000128 | 0.120969 | 0.334556 | 0.495026 | 0.007578 | 0.260059 | 0.250736 | 0.071754 | 0.015086 | 1.186947 |
| 0.3 | 0.000613 | 0.134327 | 0.254264 | 0.582265 | 0.007960 | 0.249488 | 0.235824 | 0.064565 | 0.011627 | 1.283069 |
| 0.4 | 0.000233 | 0.086125 | 0.259538 | 0.406030 | 0.007620 | 0.237060 | 0.219329 | 0.057114 | 0.008617 | 1.381131 |
| 0.5 | 0.000529 | 0.018412 | 0.283458 | 0.116434 | 0.006684 | 0.222217 | 0.200816 | 0.049309 | 0.006048 | 1.481185 |
| 0.6 | 0.007453 | 0.005468 | 0.280586 | 0.070610 | 0.005168 | 0.204059 | 0.179625 | 0.041037 | 0.003919 | 1.583190 |
| 0.7 | 0.007135 | 0.002747 | 0.271297 | 0.055117 | 0.002861 | 0.181002 | 0.154644 | 0.032158 | 0.002236 | 1.686947 |
| 0.8 | 0.003942 | 0.001296 | 0.222135 | 0.036842 | 0.000000 | 0.152068 | 0.125377 | 0.022516 | 0.001009 | 1.791966 |
| 0.9 | 0.001345 | 0.000358 | 0.154762 | 0.018222 | 0.088522 | 1.623077 | 1.178358 | 0.109412 | 0.000257 | 1.897163 |

1. The same circulation: (1,0)-(1,0)

For $\gamma = 0$, the dynamics must be equivalent to that of a single component BECs, because the two components are completely decoupled. Namely, for vortices with the same circulation (1,0)-(1,0) or (-1,0)-(-1,0), the two vortices make a circular motion. This is actually reproduced in the simulation. With increasing the initial separation R , the rotation frequency becomes smaller as shown in Fig. 10 (a).

For $\gamma \neq 0$, the vortex dynamics is influenced by the intercomponent interaction when the initial separation R is small as shown in Fig. 10(a). Although the vortices also make a circular motion, its rotation frequency has a γ -dependence, as shown in Fig. 10(b), where we plot a rotation frequency for $R = 3$ as a function of γ . The rotation frequency is slightly increased with changing the γ from zero to negative values. On the other hand, it decreases with increasing γ to positive values.

2. The different circulation: (1,0)-(-1,0)

Next, we prepare the initial state as (1,0)-(-1,0), i.e., vortex dipoles in the ψ_1 -component, and simulate the vortex trajectories for several γ , which are shown in Fig. 11. For $\gamma = 0$ as well as a single-component BEC, they move to the same direction by keeping its separation between them. For $\gamma < 0$, they move by a similar way as seen in $\gamma = 0$ (not shown). However a significant difference can be seen for $\gamma \geq 0.7$. Although the two vortices move to the same direction, they approach to each other and eventually collide to cause pair annihilation, as seen in Fig. 11. For all the values of γ , the initial velocity of the vortices does not change so much, which can be seen

in Fig. 9(b) in which the curvature of the potential for different γ does not change around $R = 3$.

C. Analysis by point vortex approximation

When we apply the simple Abrikosov ansatz of Eq. (35) and the adiabatic approximation for the wave function, we can derive the Euler-Lagrange equations similar to Eqs. (28)-(31). Here, the intervortex potential V_{12} should be replaced by that shown in Fig. 9 for (1,0)-(± 1 ,0) case. The typical solution has the same form with Eq. (32) for (1,0)-(1,0) and Eq. (33) for (1,0)-(-1,0). Since the intervortex potential has a γ -dependence within a short range of R as in Fig. 9, we expect some quantitative change of the velocity of motion. The rotation frequencies for $R = 3$ obtained by the intervortex potential V_{12} are shown in Fig. 9(b). The two methods, simple- and improved-Abrikosov ansatz can predict correct rotation frequency for the range $-1 \leq \gamma \leq 0.2$. As γ increases further, the simple Abrikosov ansatz yields unreliable result for $\gamma \geq 0.7$, which means the breakdown of this, see ansatz Fig. 10 (c). The improved method can reproduce the decreasing behavior even for $\gamma > 0.7$, but the result is not agreed quantitatively. Although there is a local minimum in V_{12} around $R = 0$ for $\gamma > 0.7$ in the latter method, the numerical simulations show that two vortices do not exhibit such an attracting behavior even at $\gamma = 0.9$ [31]. Thus, the improved ansatz Eqs. (36) and (37) is better than the simple Abrikosov ansatz but it cannot be applicable for $0.7 < \gamma < 1$. Since Eqs. (36) and (37) only consider the deformation of the amplitude of the wave function, more proper ansatz including the deformation of the phase field might improve the quantitative prediction.

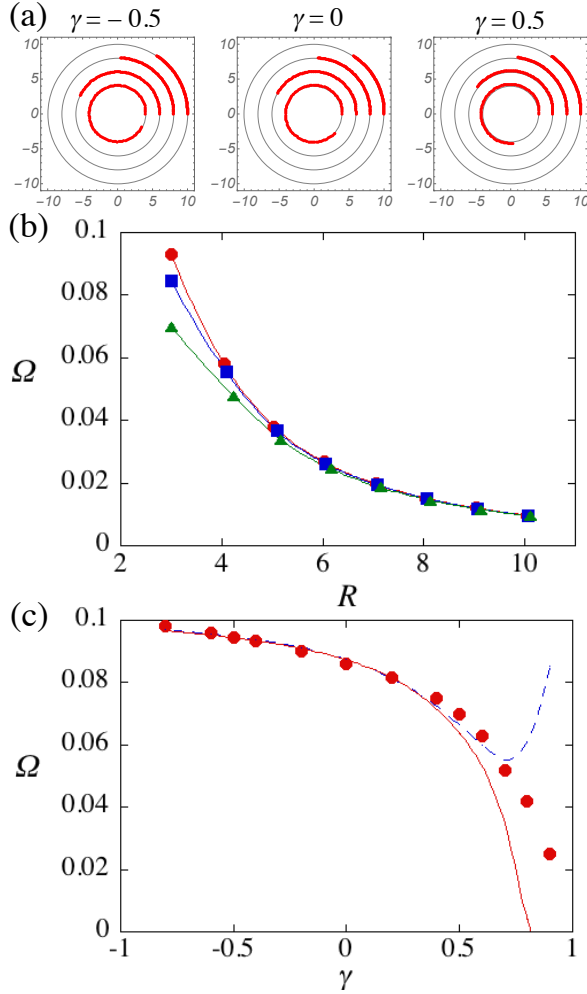


FIG. 10. (Color online) Vortex dynamics of two corotating vortices in the ψ_1 -component $(1,0)$ - $(1,0)$. (a) Trajectories of one of the vortices initially positioned at $x = +R$ for $\gamma = -0.5, 0, 0.5$ from left to right. Circles with the radius $R = 4, 6, 8, 10$ are represented by black solid curves, and the vortex trajectory from $t = 0$ to $t = 100$ are by red bold curves. (b) Plots of the rotation frequency Ω as a function of the vortex separation R for $\gamma = 0$ (squares), 0.5 (triangles), and -0.5 (circles). (c) Plots Ω as a function of γ for $R = 3$. The numerical results are compared with the two methods to calculate V_{12} : simple Abrikosov ansatz (dashed-curve) and improved Abrikosov ansatz (solid-curve).

V. SUMMARY AND DISCUSSION

In this paper, we have discussed the intervortex interaction and the dynamics of two HQVs in two-component BECs. The direct numerical simulations of the GP equations reveal nontrivial vortex dynamics as shown in Fig. 3-6, which are quite different from those in a single-component BEC. The intervortex interaction can be represented very well by the asymptotic form derived by Eto *et al.* even when the vortices are not far from each other. In our model, the vortex dynamics can be described by

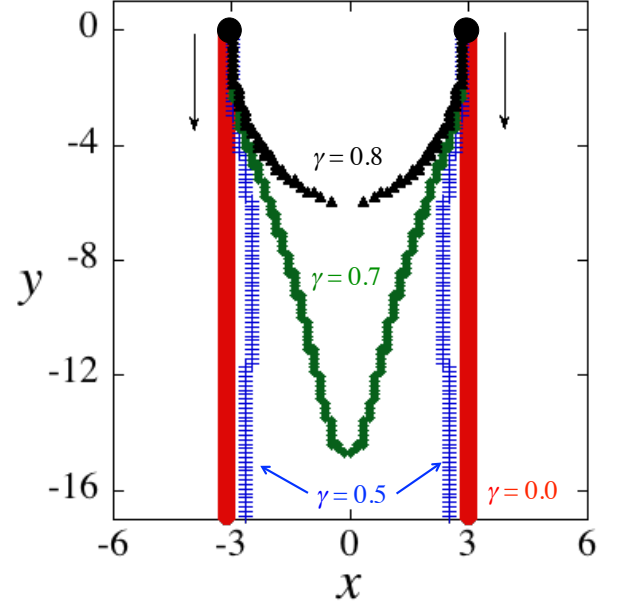


FIG. 11. The dynamical trajectories of vortex dipoles prepared initially in the ψ_1 -component, where we put a vortex at $x = R$ and an anti-vortex at $x = -R$ with $R = 3$. The (red) circles, (blue) cross, (green) diamonds, and (black) triangles represent the results for $\gamma = 0, 0.5, 0.7$, and 0.8 , respectively.

a balance between the Magnus force and the intervortex force. Through the proper treatment to estimate the intervortex force, the initial stage of the observed dynamics can be explained by this picture.

However, some of the qualitative behaviors of the vortex motion have not been explained yet. In the $(1,0)$ - $(0,\pm 1)$ case, since the vortices tend to go away from or approach to each other when the intervortex interaction is repulsive or attractive, respectively, the dynamics is similar to those of vortices in relativistic theory [32], where the time derivative of the equation of motion is second order. If there are second-order time derivative terms in the left-hand-sides of Eqs. (28)-(31), whose coefficients may be referred to as “effective vortex mass”, vortex dynamics can obtain an acceleration caused by intervortex force. We need more consideration to clarify whether the problem is solved by including these terms, and how these terms can be derived. Note that Nakamura *et al.* obtained the vortex mass by introducing the additional degrees of freedom in the phase of the condensate wave function [26]. A proper treatment of the phase dynamics might give rise to the expected mass term in the equation of motion.

Also for $(1,0)$ - $(-1,0)$ case, the vortex point model cannot explain the approaching trajectories of the vortices seen in Fig. 11. We may have some conjectures from the numerical observations. As seen in Sec. III B, it is likely that the vortices tend to approach due to the

attractive interaction between the vortices. This fact implies that the vortex might get an effective mass, which involves the acceleration of the motion. Another possibility is that the vortex motion seems to be dissipated by some mechanism. In the absence of dissipation, the vortex dipole should move by keeping their separation and this is actually observed for $\gamma \leq 0$. For $\gamma > 0$ and even in the energy conserved system, effective mutual friction may occur in counterflowing two-component superfluids due to the momentum exchange between two components [33]. Then, the vortex energy can escape to a kind of compressible energy in the other component.

Since the intervortex force in two-component BECs is very weak, the vortex dynamics shown in this paper could be observable for vortices with a relatively short distance. The number density 10^{13} - 10^{15} cm $^{-3}$ in typical cold atom experiments yields $\xi \sim 0.1$ μ m and $\tau \sim 0.1$ msec. Thus, for the vortex separation $R \leq 5$ simulated in this paper the typical time scale of the vortex dynamics such as the period of the circular motion is order of 10^{2-3} msec. Much longer time is needed to detect the dynamics of initially well-separated vortices with $R \geq 6$; for example, according to Fig. 7(a), the period of the circular motion is about 2 sec for $R = 6$ and 6 sec for $R = 8$. Also, when the condensate is trapped by a harmonic potential, the vortex exhibits a precession motion around the center due to the density inhomogeneity [11]. This frequency is proportional to the inverse of the square of the Thomas-Fermi radius. It is necessary to prepare condensates with large Thomas-Fermi radius to verify our prediction.

Half-quantized vortices in two-component BECs are predicted to exhibit exotic vortex lattice structures in the presence of the coherent Rabi coupling between the two components [10, 34]. The interaction and dynamics of half-quantized vortices in the presence of the Rabi coupling are also an important future problem.

Generalization of our result to fractional vortices in multi-component more than two components [35, 36] is straightforward. Finally, the method introduced in this paper should be applicable to different systems such as fractional non-Abelian vortices in dense quark matter [37], for which the interaction between two well-separated vortices is the same with that of superfluid vortices [38]. The short range interaction is important to determine the vortex lattice structure [39].

ACKNOWLEDGMENTS

The work of K. K. is supported by KAKENHI from the Japan Society for the Promotion of Science (JSPS) Grant-in-Aid for Scientific Research (KAKENHI Grant No. 26400371). The work of M. E. is supported in part by JSPS Grant-in-Aid for Scientific Research (KAKENHI Grant No. 26800119). The work of M. N. is supported in part by JSPS Grant-in-Aid for Scientific Research (KAKENHI Grant No. 25400268) and by a Grant-in-Aid for Scientific Research on Innovative Areas “Topological Ma-

terials Science” (KAKENHI Grant No. 15H05855) and “Nuclear Matter in Neutron Stars Investigated by Experiments and Astronomical Observations” (KAKENHI Grant No. 15H00841) from the the Ministry of Education, Culture, Sports, Science (MEXT) of Japan. The work of M. E. and M. N. is also supported in part by the MEXT-Supported Program for the Strategic Research Foundation at Private Universities “Topological Science” (Grant No. S1511006).

Appendix A: Derivation of the equation of motion for vortex coordinates

Here, we describe a derivation of the equation of motion for the vortex coordinates. For the $(1, 0)$ - $(0, \pm 1)$ case in Sec. III, the wave functions for the two-component BECs are approximately written as Eqs. (21)-(25). The time evolution of the system is only included in the coordinates $\mathbf{r}_1(t)$ and $\mathbf{r}_2(t)$ in the adiabatic limit. The Lagrangian is given by Eq. (27), and the total energy $E_0^{(q_1, q_2)}$ [Eq. (18)] is reduced to the vortex-vortex interaction V_{12} shown in Fig. 2 after substituting Eqs. (21)-(25) and making the integration.

By taking the variation of the action $S = \int dt L$ with respect to \mathbf{r}_i , we obtain

$$\begin{aligned} \delta S = & - \sum_i \int dt \left\{ \int d\mathbf{r} \left[\dot{\theta}_i (\nabla_i \rho_i) + \rho_i (\nabla_i \dot{\theta}_i) \right. \right. \\ & \left. \left. + \dot{\theta}_{\bar{i}} (\nabla_{\bar{i}} \rho_{\bar{i}}) \right] + \nabla_i V_{12} \right\} \cdot \delta \mathbf{r}_i \\ & - \sum_i \int dt \int d\mathbf{r} \rho_i (\nabla_i \theta_i) \cdot \delta \dot{\mathbf{r}}_i, \end{aligned} \quad (\text{A1})$$

where $i = 1, 2$, $\bar{i} = 2(1)$ when $i = 1(2)$, and $\nabla_i \equiv \nabla_{\mathbf{r}_i}$. After integrating partly, the last term in Eq. (A1) becomes

$$\int dt \int d\mathbf{r} (\dot{\rho}_i \nabla_{\mathbf{r}_i} \theta_i + \rho_i \nabla_{\mathbf{r}_i} \dot{\theta}_i) \cdot \delta \mathbf{r}_i. \quad (\text{A2})$$

Thus, the second term of Eq. (A1) and that of Eq. (A2) are canceled out, so that we get

$$\begin{aligned} \delta S = & - \sum_i \int dt \left\{ \int d\mathbf{r} \left[\dot{\theta}_i (\nabla_i \rho_i) - \dot{\rho}_i (\nabla_i \theta_i) \right. \right. \\ & \left. \left. + \dot{\theta}_{\bar{i}} (\nabla_{\bar{i}} \rho_{\bar{i}}) \right] + \nabla_i V_{12} \right\} \cdot \delta \mathbf{r}_i. \end{aligned} \quad (\text{A3})$$

According to Eqs. (22)-(25), we have the relation

$$\begin{aligned} \dot{\rho}_i &= (\nabla_i \rho_i) \cdot \dot{\mathbf{r}}_i + (\nabla_{\bar{i}} \rho_i) \cdot \dot{\mathbf{r}}_{\bar{i}}, \\ \dot{\theta}_i &= (\nabla_i \theta_i) \cdot \dot{\mathbf{r}}_i, \end{aligned} \quad (\text{A4})$$

and δS can be written as

$$\begin{aligned} \delta S = & - \sum_i \int dt \left\{ \int d\mathbf{r} \left[(\nabla_i \theta_i) \cdot \dot{\mathbf{r}}_i (\nabla_i \rho_i) \right. \right. \\ & - (\nabla_i \rho_i) \cdot \dot{\mathbf{r}}_i (\nabla_i \theta_i) - (\nabla_{\bar{i}} \rho_i) \cdot \dot{\mathbf{r}}_{\bar{i}} (\nabla_i \theta_i) \\ & \left. \left. + (\nabla_{\bar{i}} \theta_i) \cdot \dot{\mathbf{r}}_{\bar{i}} (\nabla_i \rho_i) \right] + \nabla_i V_{12} \right\} \cdot \delta \mathbf{r}_i. \end{aligned} \quad (\text{A5})$$

By using the formula $(\mathbf{A} \times \mathbf{B}) \cdot (\mathbf{C} \times \mathbf{D}) = (\mathbf{A} \cdot \mathbf{C})(\mathbf{B} \cdot \mathbf{D}) - (\mathbf{A} \cdot \mathbf{D})(\mathbf{B} \cdot \mathbf{C})$, the first two terms can be written as

$$\int d\mathbf{r} (\nabla_i \rho_i \times \nabla_i \theta_i) \cdot (\delta \mathbf{r}_i \times \dot{\mathbf{r}}_i). \quad (\text{A6})$$

Here, we note that $\nabla_{\mathbf{r}_i}$ can be replaced by $-\nabla$ when it acts on $\mathbf{r} - \mathbf{r}_i$. Then, $\nabla_i \rho_i = -\nabla \rho_i - \nabla_{\bar{i}} \rho_i$ and $\nabla_i \theta_i = -\nabla \theta_i$. Equation (A6) becomes

$$\int d\mathbf{r} [(\nabla \rho_i \times \nabla \theta_i) - (\nabla_{\bar{i}} \rho_i \times \nabla_i \theta_i)] \cdot (\delta \mathbf{r}_i \times \dot{\mathbf{r}}_i). \quad (\text{A7})$$

The first term can be written as

$$\begin{aligned} & - \int d\mathbf{r} [(\nabla \rho_i \times \nabla \theta_i) \times \dot{\mathbf{r}}_i] \cdot \delta \mathbf{r}_i \\ & = - \int d\mathbf{r} [\nabla \times (\rho_i \nabla \theta_i) \times \dot{\mathbf{r}}_i] \cdot \delta \mathbf{r}_i. \end{aligned} \quad (\text{A8})$$

The spatial integral can be calculated by the Stokes theorem as

$$- 2\pi q_i \rho_{r=\infty} \hat{\mathbf{z}} \times \dot{\mathbf{r}}_i \cdot \delta \mathbf{r}_i. \quad (\text{A9})$$

This term represents the well-known Magnus force. It should be noted that we still remain some integrals: (i) the third and fourth terms of Eq. (A5)

$$\int d\mathbf{r} \left\{ [(\nabla_{\bar{i}} \theta_i) \cdot \dot{\mathbf{r}}_{\bar{i}}] (\nabla_i \rho_{\bar{i}}) - [(\nabla_{\bar{i}} \rho_i) \cdot \dot{\mathbf{r}}_{\bar{i}}] (\nabla_i \theta_i) \right\} \cdot \delta \mathbf{r}_i, \quad (\text{A10})$$

and (ii) the second term of Eq. (A7)

$$\int d\mathbf{r} \left\{ [(\nabla_i \theta_i) \cdot \dot{\mathbf{r}}_i] (\nabla_{\bar{i}} \rho_i) - [(\nabla_{\bar{i}} \rho_i) \cdot \dot{\mathbf{r}}_i] (\nabla_i \theta_i) \right\} \cdot \delta \mathbf{r}_i. \quad (\text{A11})$$

These integrals consist of cross terms of the gradient of the density or the phase at the different position vectors, which may be a small contribution for the integration due to the small overlap for well separated vortices. As seen in the Appendix B, these terms give a minor contribution to the motion of point vortices without any change of the qualitative behaviors.

Since $\rho_{r=\infty} = 1$ in our unit, the equation of motion is written by

$$\begin{aligned} 2\pi q_i \dot{\mathbf{r}}_i \times \hat{\mathbf{z}} = & -\nabla_i V_{12} \\ & + \int d\mathbf{r} \left[(\nabla_{\bar{i}} \rho_i) \cdot \dot{\mathbf{r}}_{\bar{i}} (\nabla_i \theta_i) - (\nabla_{\bar{i}} \theta_i) \cdot \dot{\mathbf{r}}_{\bar{i}} (\nabla_i \rho_i) \right] \\ & + \int d\mathbf{r} \left[(\nabla_i \theta_i) \cdot \dot{\mathbf{r}}_i (\nabla_{\bar{i}} \rho_i) - (\nabla_{\bar{i}} \rho_i) \cdot \dot{\mathbf{r}}_i (\nabla_i \theta_i) \right]. \end{aligned} \quad (\text{A12})$$

By neglecting the last two integrals, we arrive at Eqs. (28)-(31)

Following the same procedure, we can also derive the equations of motion for the $(1,0)$ - $(\pm 1,0)$ case. The ansatz is given by Eqs. (35). The variation of the action becomes

$$\begin{aligned} \delta S = & \sum_i \int dt \left\{ \int d\mathbf{r} \left[(\nabla_i \rho_1) \dot{\theta}_1 - \dot{\rho}_1 (\nabla_i \theta_1) \right] \right. \\ & \left. - \nabla_i V_{12} \right\} \cdot \delta \mathbf{r}_i. \end{aligned} \quad (\text{A13})$$

Using the relations

$$\begin{aligned} \dot{\rho}_1 &= (\nabla_1 \rho_1) \cdot \dot{\mathbf{r}}_1 + (\nabla_2 \rho_1) \cdot \dot{\mathbf{r}}_2, \\ \dot{\theta}_1 &= (\nabla_1 \theta_1) \cdot \dot{\mathbf{r}}_1 + (\nabla_2 \theta_1) \cdot \dot{\mathbf{r}}_2, \end{aligned} \quad (\text{A14})$$

we get

$$\begin{aligned} \delta S = & - \sum_i \int dt \left\{ \nabla_i V_{12} \right. \\ & + \int d\mathbf{r} [(\nabla_i \theta_1) \cdot \dot{\mathbf{r}}_i (\nabla_i \rho_1) - (\nabla_i \rho_1) \cdot \dot{\mathbf{r}}_i (\nabla_i \theta_1)] \\ & \left. + \int d\mathbf{r} [(\nabla_{\bar{i}} \theta_1) \cdot \dot{\mathbf{r}}_{\bar{i}} (\nabla_i \rho_1) - (\nabla_{\bar{i}} \rho_1) \cdot \dot{\mathbf{r}}_{\bar{i}} (\nabla_i \theta_1)] \right\} \cdot \delta \mathbf{r}_i. \end{aligned} \quad (\text{A15})$$

The integral in the second line gives the Magnus force term as well as the additional integral similar to Eq. (A11), where we use the replacement $\nabla_i \rho_1 = -\nabla \rho_1 - \nabla_{\bar{i}} \rho_1$ and $\nabla_i \theta_1 = -q_i \nabla \theta^0(\mathbf{r} - \mathbf{r}_i)$. The integral in the third line also provides additional contribution similar to Eq. (A10). There is a difference from the $(1,0)$ - $(0,\pm 1)$ case in the additional integrals, where the gradient of the density is written by the core profile $f(\mathbf{r})$ instead of the hump profile $h(\mathbf{r})$. These are generally neglected in the analysis of a single-component superfluid [12–14] as well as our analysis in the text. The equation of motion is given by

$$\begin{aligned} 2\pi q_i \dot{\mathbf{r}}_i \times \hat{\mathbf{z}} = & -\nabla_i V_{12} \\ & + \int d\mathbf{r} \left[(\nabla_{\bar{i}} \rho_1) \cdot \dot{\mathbf{r}}_{\bar{i}} (\nabla_i \theta_1) - (\nabla_{\bar{i}} \theta_1) \cdot \dot{\mathbf{r}}_{\bar{i}} (\nabla_i \rho_1) \right] \\ & + \int d\mathbf{r} \left[(\nabla_i \theta_1) \cdot \dot{\mathbf{r}}_i (\nabla_{\bar{i}} \rho_1) - (\nabla_{\bar{i}} \rho_1) \cdot \dot{\mathbf{r}}_i (\nabla_i \theta_1) \right]. \end{aligned} \quad (\text{A16})$$

Appendix B: Contribution of the additional integrals: Eqs. (A10) and (A11)

Here, we discuss the additional contributions Eqs. (A10) and (A11) shown in the previous derivation. We focus on the $(1,0)$ - $(0,\pm 1)$ vortex state for explanation, but it is essentially the same for the $(1,0)$ - $(\pm 1,0)$ case.

With remaining these additional terms, the equations of motion can be written as

$$(2\pi - I_0)q_1\dot{y}_1 = -\frac{\partial V_{12}}{\partial x_1} - I_{xx}\dot{x}_2 - I_{xy}\dot{y}_2, \quad (\text{B1})$$

$$-(2\pi - I_0)q_1\dot{x}_1 = -\frac{\partial V_{12}}{\partial y_1} - I_{yx}\dot{x}_2 - I_{yy}\dot{y}_2, \quad (\text{B2})$$

$$(2\pi - I_0)q_2\dot{y}_2 = -\frac{\partial V_{12}}{\partial x_2} + I_{xx}\dot{x}_1 + I_{xy}\dot{y}_1, \quad (\text{B3})$$

$$-(2\pi - I_0)q_2\dot{x}_2 = -\frac{\partial V_{12}}{\partial y_2} + I_{xy}\dot{x}_1 + I_{yy}\dot{y}_1. \quad (\text{B4})$$

The coefficients I_0 and $I_{\alpha\beta}$ ($\alpha, \beta = x, y$) are given by

$$I_0 = \int d\mathbf{r} \left[-f(\mathbf{r} - \mathbf{r}_1)v_x^0(\mathbf{r} - \mathbf{r}_1)\partial_y h(\mathbf{r} - \mathbf{r}_2) + f(\mathbf{r} - \mathbf{r}_1)v_y^0(\mathbf{r} - \mathbf{r}_1)\partial_x h(\mathbf{r} - \mathbf{r}_2) \right], \quad (\text{B5})$$

$$I_{\alpha\beta} = \int d\mathbf{r} \left[-q_1 f(\mathbf{r} - \mathbf{r}_1)v_\alpha^0(\mathbf{r} - \mathbf{r}_1)\partial_\beta h(\mathbf{r} - \mathbf{r}_2) + q_2 f(\mathbf{r} - \mathbf{r}_2)v_\beta^0(\mathbf{r} - \mathbf{r}_2)\partial_\alpha h(\mathbf{r} - \mathbf{r}_1) \right] \quad (\text{B6})$$

with $v_\alpha^0(\mathbf{r} - \mathbf{r}_i) = \partial_\alpha \theta^0(\mathbf{r} - \mathbf{r}_i)$. The integrals I_0 and $I_{\alpha\beta}$ come from Eqs. (A11) and (A10), respectively. These are invariant under the change $q_1 \leftrightarrow q_2$ and $\mathbf{r}_1 \leftrightarrow \mathbf{r}_2$ and functions of the relative position $\mathbf{r}_{12} = \mathbf{r}_2 - \mathbf{r}_1 = (x_{12}, y_{12})$, which can be easily seen by changing the variables as $\mathbf{r} \rightarrow \mathbf{r} - \mathbf{r}_{12}/2$. The integrand consists of an overlap of the current density around \mathbf{r}_1 and the density gradient around \mathbf{r}_2 , and that of vice versa. For $\gamma = 0$, these integrals vanish because of $\nabla h = 0$. For the well separated vortices, the overlap should be small. For short-distance dynamics, however, these integrals may have some contribution. The typical values of I_0 and $I_{\alpha\beta}$ as functions of x_{12} and y_{12} for $\gamma = \pm 0.5$ are shown in Fig. 12, which are calculated by the numerical integral with the approximated form Eqs. (14), (15), and (26) of the wave function. As seen in Eqs. (B5) and (B6), $I_{xy} = I_0$ if $q_1 = q_2$ (the second integrals of Eqs. (B5) and (B6) are equivalent under $\mathbf{r}_1 \leftrightarrow \mathbf{r}_2$). We remain these terms here, finding that there are only small correction of the quantitative dynamical feature without the change of the qualitative dynamics.

Let us see the impact of these terms to the equations of motion. For $(1,0)-(0,1)$ [$(q_1, q_2) = (1, 1)$], the integral becomes $I_0 = I_{xy}$, $I_{xx} = I_{yy} = 0$, and $I_{yx} = -I_{xy}$ because of the inversion symmetry $\mathbf{r}_1 \leftrightarrow \mathbf{r}_2$. Moreover, I_{xy} is a isotropic function of \mathbf{r}_{12} , being written as $I_{xy}(r_{12})$. Since \mathbf{r}_{12} is still a constant of motion even in the presence of I_{xy} , I_{xy} and I_0 are constants determined by the initial position of the vortices. We obtain the equation of motion for \mathbf{r}_i as

$$\ddot{\mathbf{r}}_i = - \left[\frac{2}{(2\pi - I_0 - I_{xy})r_{12}} \frac{\partial V_{12}}{\partial r_{12}} \right]^2 \mathbf{r}_i. \quad (\text{B7})$$

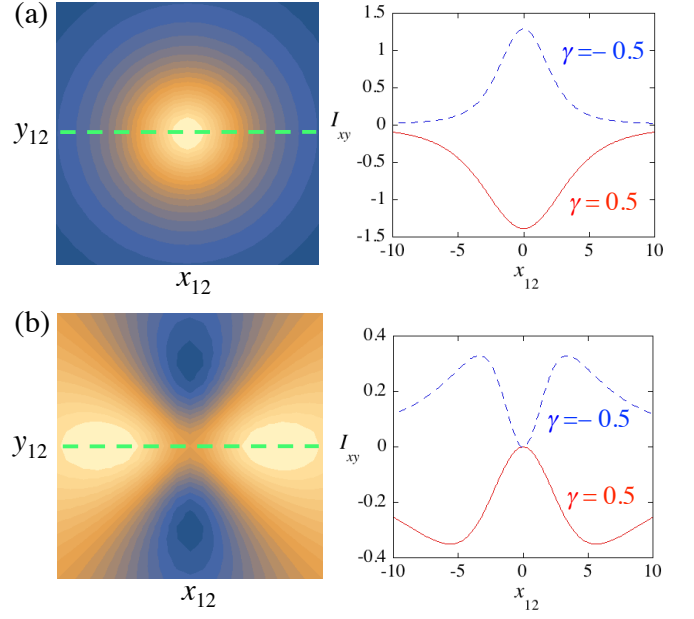


FIG. 12. (Color online) Typical profiles of the integrals (a) I_{xy} and I_0 ($I_{xy} = I_0$) for $(1,0)-(0,1)$ and (b) I_{xy} for $(1,0)-(0,-1)$. The left panels show the contourplots of I_{xy} for $\gamma < 0$; for $\gamma > 0$ the sign of I_{xy} is inverted from that of $\gamma < 0$. The value is larger (smaller) in the brighter (darker) region. In the right panel, we plot the cross section of I_{xy} along the $y_{12} = 0$ line for $\gamma = 0.5$ and -0.5 .

This gives an uniform circular motion and the rotation frequency depends on the γ . The factor $I_0 + I_{xy}$ only modifies the rotation frequency as a function of r_{12} .

For $(1,0)-(0,-1)$ [$(q_1, q_2) = (1, -1)$], the inversion symmetry $\mathbf{r}_1 \leftrightarrow \mathbf{r}_2$ leads to $I_{xx} = -I_{yy}$ and $I_{yx} = I_{xy}$, but I_0 is not equal to I_{xy} . Even with this additional terms, one can show that \mathbf{r}_{12} is a constant of motion. An appropriate choice of the initial condition, such as $x_{12}(0) = 2R$ and $y_{12}(0) = 0$ as in our simulations, makes I_{xx} vanish and I_{xy} being constant determined by the initial condition. The solution is given by $x_{1(2)} = (-)R$ and

$$y_1 = y_2 = \frac{1}{2\pi - I_0 - I_{xy}} \left(\frac{\partial V_{12}}{\partial r_{12}} \right) t. \quad (\text{B8})$$

This is exactly an uniform linear motion for the both vortices.

In both cases, Eqs. (B7) and (B8) imply that I_0 and I_{xy} do not change any qualitative behavior of the vortex dynamics, but the initial velocity of the vortices can be modified through the factor $2\pi - I_0 - I_{xy}$. The quantitative correction due to I_0 and I_{xy} is very small, except for $|x_{12}| < 5$ ($R < 2.5$) in the $(1,0)-(0,1)$ case where $I_{xy} \sim \mathcal{O}(1)$ [Fig. 12(a)]. However, when we take account of the small correction, the initial velocity obtained from the GP simulations in Fig. 7 is explained better. Figure 13 shows the initial velocity of the GP equations in

Fig. 7 again as well as that obtained from the intervortex potential Eq. (19) including the correction I_{xy} . The correction is included in a different way for $(1,0)$ -($0,1$) and $(1,0)$ -($0,-1$) case as seen in Fig. 12; for $\gamma > 0$ the initial velocity of $(1,0)$ -($0,1$) is slightly smaller than that of $(1,0)$ -($0,-1$), and vice versa for $\gamma < 0$. This is actually observed in the numerical results.

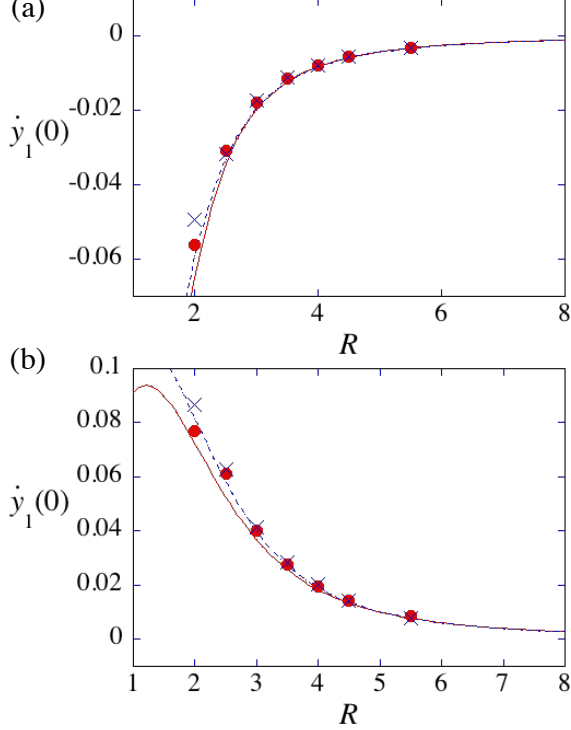


FIG. 13. A similar plots with Fig. 7, but the numerical results are compared with the initial velocity calculated from the intervortex force with the correction of I_0 and I_{xy} for (a) $\gamma = -0.5$ and (b) $\gamma = 0.5$. The (red) circles and (blue) crosses represent the numerical results of the GP equation for $(1,0)$ -($0,1$) and $(1,0)$ -($0,-1$), respectively. The solid and dashed curves represent $(\partial V_{12}/\partial r_{12})/(2\pi - I_0 - I_{xy})$ for $(1,0)$ -($0,1$) and $(1,0)$ -($0,-1$), respectively.

For the $(1,0)$ and $(\pm 1,0)$ case, the integrals I_0 and $I_{\alpha\beta}$ are given by

$$I_0 = \int d\mathbf{r} \left[-f(\mathbf{r} - \mathbf{r}_1) v_x^0(\mathbf{r} - \mathbf{r}_1) \partial_y f(\mathbf{r} - \mathbf{r}_2) + f(\mathbf{r} - \mathbf{r}_1) v_y^0(\mathbf{r} - \mathbf{r}_1) \partial_x f(\mathbf{r} - \mathbf{r}_2) \right],$$

$$I_{\alpha\beta} = \int d\mathbf{r} \left[-q_1 f(\mathbf{r} - \mathbf{r}_1) v_\alpha^0(\mathbf{r} - \mathbf{r}_1) \partial_\beta f(\mathbf{r} - \mathbf{r}_2) + q_2 f(\mathbf{r} - \mathbf{r}_2) v_\beta^0(\mathbf{r} - \mathbf{r}_2) \partial_\alpha f(\mathbf{r} - \mathbf{r}_1) \right]. \quad (\text{B9})$$

The difference from Eq. (B6) is that the density gradient is altered by the vortex core profile $f(\mathbf{r})$ instead of the hump profile $h(\mathbf{r})$. These coefficients can be also calculated by the numerical integrals, and the overall profile is consistent with those in Fig. 12, except its sign. The above argument is also applicable to this situation because the equation of motion is essentially identical to Eqs. (B1)-(B4).

-
- [1] G. E. Volovik, *The Universe in a Helium Droplet* (Oxford University Press, New York, 2003).
 - [2] E. Babaev, Phys. Rev. Lett. **89** (2002) 067001; E. Babaev, A. Sudbo and N. W. Ashcroft, Nature **431**, 666 (2004); J. Smiseth, E. Smorgrav, E. Babaev and A. Sudbo, Phys. Rev. B **71**, 214509 (2005); E. Babaev and N. W. Ashcroft, Nature Phys. **3**, 530 (2007).
 - [3] V. P. Mineev, Low Temp. Phys. **39**, 818 (2013).
 - [4] J. Jang, D. G. Ferguson, V. Vakaryuk, R. Budakian, S. B. Chung, P. M. Goldbart, Y. Maeno, Science **331**, 186 (2011).
 - [5] K. G. Lagoudakis, T. Ostatnický, A. V. Kavokin, Y. G. Rubo, R. André, B. Deveaud-Plédran, Science **326**, 974 (2009).
 - [6] F. Manni, K. G. Lagoudakis, T. C. H. Liew, R. André, V. Savona and B. Deveaud, Nat. Comm. **3**, 1309 (2012).
 - [7] S. W. Seo, S. Kang, W. J. Kwon, and Y.-I. Shin, Phys. Rev. Lett. **115**, 015301 (2015).
 - [8] S. Autti, V. V. Dmitriev, V. B. Eltsov, J. Makinen, G. E. Volovik, A. N. Yudin, V. V. Zavjalov, arXiv:1508.02197 [cond-mat.other].
 - [9] U. Leonhardt and G. E. Volovik, JETP Lett. **72**, 46 (2000).
 - [10] K. Kasamatsu, M. Tsubota and M. Ueda, Int. J. Mod. Phys. B **19**, 1835 (2005).
 - [11] A. L. Fetter, Rev. Mod. Phys. **81**, 647 (2009).
 - [12] D. V. Freilich, D. M. Bianchi, A. M. Kaufman, T. K. Langin, and D. S. Hall, Science **329**, 1182 (2010).

- [13] S. Middelkamp, P. J. Torres, P. G. Kevrekidis, D. J. Frantzeskakis, R. Carretero-Gonzalez, P. Schmelcher, D. V. Freilich, D.S. Hall, Phys. Rev. A **84** 011605(R) (2011).
- [14] R. Navarro, R. Carretero-González, P. J. Torres, P. G. Kevrekidis, D. J. Frantzeskakis, M. W. Ray, E. Altuntas, and D. S. Hall, Phys. Rev. Lett. **110**, 225301 (2013).
- [15] D. M. Jezek, P. Capuzzi, and H. M. Cataldo, Phys. Rev. A **64**, 023605 (2001).
- [16] E. J. Mueller and T.-L. Ho, Phys. Rev. Lett. **88**, 180403 (2002).
- [17] K. Kasamatsu, M. Tsubota, and M. Ueda, Phys. Rev. Lett. **91**, 150406 (2003).
- [18] G. Catelani and E. A. Yuzbashyan, Phys. Rev. A **81**, 033629 (2010).
- [19] M. R. Matthews, B. P. Anderson, P. C. Haljan, D. S. Hall, C. E. Wieman, and E. A. Cornell, Phys. Rev. Lett., **83**, 2498 (1999).
- [20] M. Eto, K. Kasamatsu, M. Nitta, H. Takeuchi, M. Tsubota, Phys. Rev. A **83** 063603 (2011).
- [21] C. J. Pethick and H. Smith, *Bose-Einstein Condensation in Dilute Gases, 2nd ed.* (Cambridge University Press, New York, 2008).
- [22] A. Aftalion, P. Mason, and J. Wei, Phys. Rev. A **85**, 033614 (2012).
- [23] W. E. Shirley, B. M. Anderson, C. W. Clark, and R. M. Wilson, Phys. Rev. Lett. **113**, 165301 (2014).
- [24] D. S. Dantas, A. R. P. Lima, A. Chaves, C. A. S. Almeida, G. A. Farias, and M. V. Milošević, Phys. Rev. A **91**, 023630 (2015).
- [25] P. Öhberg and L. Santos, Phys. Rev. A **66**, 013616 (2002).
- [26] K. Nakamura, D. Babajanov, D. Matrasulov, M. Kobayashi, Phys. Rev. A **86**, 053613 (2012).
- [27] A. L. Gaunt, T. F. Schmidutz, I. Gotlibovych, R. P. Smith, and Z. Hadzibabic, Phys. Rev. Lett. **110**, 200406 (2013).
- [28] P. Mason, Phys. Rev. A **88**, 043608 (2013).
- [29] We made similar calculations by using the Dirichlet boundary condition and confirmed that the results are same as those done by the Neumann condition. We also confirm that the boundary effect is negligible by seeing that a single vortex at some position does not move.
- [30] L. Jacobs and C. Rebbi, Phys. Rev. B **19**, 4486 (1979).
- [31] We confirmed that for $\gamma = 0.9$ two initially close vortices move so as to repel each other through the imaginary time evolution.
- [32] N. Manton and P. Sutcliffe, *Topological Solitons* (Cambridge University Press, New York, 2007).
- [33] H. Takeuchi, S. Ishino, and M. Tsubota, Phys. Rev. Lett. **105**, 205301 (2010).
- [34] M. Cipriani and M. Nitta, Phys. Rev. Lett. **111**, 170401 (2013).
- [35] M. Cipriani and M. Nitta, Phys. Rev. A **88**, 013634 (2013).
- [36] M. Eto and M. Nitta, Phys. Rev. A **85**, 053645 (2012); M. Eto and M. Nitta, Europhys. Lett. **103**, 60006 (2013).
- [37] M. Eto, Y. Hirono, M. Nitta and S. Yasui, PTEP **2014**, no. 1, 012D01 (2014).
- [38] E. Nakano, M. Nitta and T. Matsuura, Phys. Rev. D **78**, 045002 (2008).
- [39] M. Kobayashi, E. Nakano and M. Nitta, JHEP **1406**, 130 (2014).